

Experimentally Feasible Dynamical Casimir Effect in Parametrically Amplified Cavity Optomechanics

Wei Qin,¹ Vincenzo Macrì,¹ Adam Miranowicz,^{1,2} Salvatore Savasta,^{1,3} and Franco Nori^{1,4}

¹*Theoretical Quantum Physics Laboratory, RIKEN Cluster for Pioneering Research, Wako-shi, Saitama 351-0198, Japan*

²*Faculty of Physics, Adam Mickiewicz University, 61-614 Poznań, Poland*

³*Dipartimento di Scienze Matematiche e Informatiche, Scienze Fisiche e Scienze della Terra, Università di Messina, I-98166 Messina, Italy*

⁴*Department of Physics, The University of Michigan, Ann Arbor, Michigan 48109-1040, USA*

We present a method for observing the dynamical Casimir effect (DCE) induced by a mechanical motion in an optomechanical system. This employs a detuned, parametric driving to squeeze a cavity mode, so that the squeezed-cavity-mode frequency is externally tunable. The mechanical mode, with a typical resonance frequency, can parametrically and resonantly couple to the squeezed cavity mode, thus leading to a resonantly amplified DCE in the squeezed frame. This process, in the laboratory frame, can also be interpreted as anti-Stokes hyper-Raman scattering. We demonstrate observable signatures of the DCE, including an output-photon flux spectrum with a resolved resonance peak, and a monotonic increase in the maxima of this peak with the strength of a mechanical driving. Furthermore, we demonstrate that for weak squeezing, the DCE can be mapped from the squeezed to the laboratory frame, which allows for a more direct DCE detection. Our method requires neither an ultra-high mechanical frequency nor an ultrastrong single-photon optomechanical coupling and, thus, could be implemented in a wide range of physical systems.

One of the most astonishing phenomena of nature, predicted by quantum field theory, is that the quantum vacuum is not empty but teems with virtual particles. Under certain external perturbations, these vacuum fluctuations could be converted into real particles by dynamical amplification mechanisms such as the Schwinger process [1], Hawking radiation [2], and Unruh effect [3]. The dynamical Casimir effect (DCE) describes the creation of photons out of the quantum vacuum due to a moving mirror [4, 5]. The physics underlying the DCE is that the electromagnetic field cannot adiabatically adapt to the time-dependent boundary condition imposed by the mechanical motion of the mirror, such that it occurs a mismatch of vacuum modes in time. This gives rise to the emission of photon pairs from the vacuum and, at the same time, to the equal-energy dissipation of the mechanical phonons. Thus, according to energy conservation, the DCE can also be understood as the energy conversion of the mechanical motion to the electromagnetic field.

In order to detect the DCE, the mirror velocity is, however, required to be close to the speed of light [6, 7]. This requirement is the main obstacle in observing the DCE in a realistic setup. This problem led to many alternative proposals, which replaced the mechanical motion with an effective motion provided by, e.g., modulating dielectric properties of semiconductors or superconductors [8–12], or modulating the ultrastrong light-matter coupling in cavity quantum electrodynamics (QED) [13–20]. In particular, two remarkable experimental partial verifications have recently been implemented utilizing a superconducting quantum interference device [7, 21–25] and a Josephson metamaterial [26], respectively, to produce the effective

motion. Despite such achievements, implementing the DCE with a massive mirror is still highly desirable for a more fundamental understanding of the DCE physics. This is because the parametric conversion of mechanical energy to photons, which is a key feature of the DCE predicted in its original proposals [4–7], can be demonstrated in this case, contrary to proposals based on the effective motion. However, owing to the serious problem mentioned above (very fast oscillating mirror), such a mechanical radiation has not yet been observed experimentally, although the DCE has been predicted for almost fifty years. Here, we propose a novel approach to this outstanding problem, and we show that in a squeezed optomechanical system, a mirror oscillating at a common frequency can induce an observable DCE.

Cavity optomechanics provides a promising platform to explore the interaction between light and mechanics [27]. The DCE can, in principle, also be directly implemented in optomechanical systems [28–34]. But it requires a mechanical frequency ω_m to be very close to the cavity frequency ω_c , or even a single-photon optomechanical coupling g_0 to reach the ultrastrong-coupling regime $g_0/\omega_m \gtrsim 0.1$ [34]. For typical parameters, $\omega_m \sim$ MHz is much smaller than $\omega_c \sim$ THz (\sim GHz) for optical (microwave) cavities, and at the same time, achieving the ultrastrong coupling is, currently, also a very challenging task in optomechanical experiments. However, as we describe in this manuscript, when squeezing the cavity [35], the squeezed-cavity-mode (SCM) frequency is tunable, such that the SCM can parametrically and resonantly couple to a mechanical mode with a typically available ω_m . This enables an observable DCE in the squeezed frame. Furthermore, for accessible values of g_0 , such a coupling can result

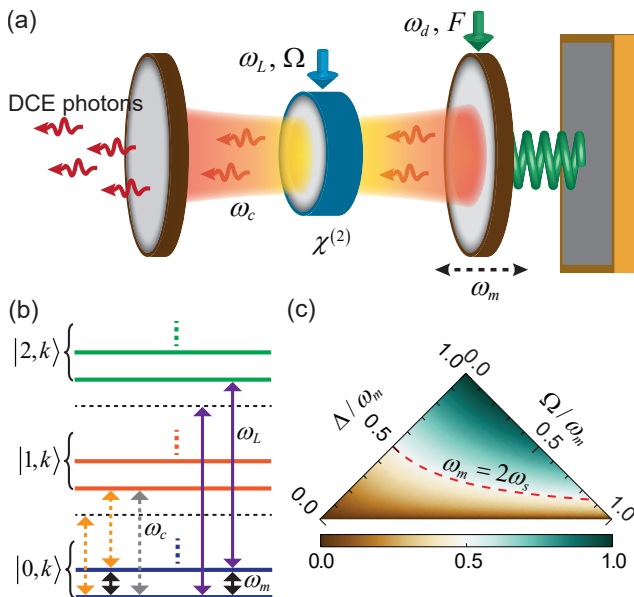


FIG. 1. (a) Setup for observing the mechanical DCE. In this optomechanical system, a $\chi^{(2)}$ nonlinear crystal driven at frequency ω_L and amplitude Ω is used to squeeze the cavity mode of frequency ω_c , and the mechanical resonator is driven by a force of frequency ω_d and amplitude F . The DCE occurs in the squeezed frame, and a large number of DCE photons, emitted from the cavity, can be observed in the laboratory frame. (b) Level diagram of the bare optomechanical system. The solid (dashed) arrows indicate two-photon hyper Raman (one-photon Raman) scattering processes induced by the optomechanical coupling. We assume, for simplicity, that $\Omega \ll \omega_m$, such that the resonance condition is $2\omega_c \simeq \omega_L + \omega_m$. (c) SCM frequency ω_s as a function of the parametric-driving detuning Δ and strength Ω . The dashed curve represents the $\omega_m = 2\omega_s$ case. Here, in order for the system to be stable, we need to have $\Delta > \Omega$.

in a measurable output-photon flux originating from the DCE.

As opposed to previous mechanical-DCE proposals, our approach requires neither an ultra-high mechanical frequency nor an ultrastrong coupling. In addition, the model discussed here is a generic optomechanical setup. Hence, with current technologies our proposal could be realized in various physical architectures, e.g., superconducting resonators [36, 37] and optical cavities [38].

Model.— We consider an optomechanical system, as schematically depicted in Fig. 1(a). Most experiments in cavity optomechanics are carried out under a *coherent optical driving* of a cavity, so that the cavity field can be split into an average coherent amplitude and a fluctuating term [27]. For a red-detuned driving, the fluctuations of the cavity field and the mechanical resonator can interchange quanta resonantly [39]. This process is viewed as one-photon Raman scattering [see Fig. 1(b)]. The basic idea underlying our proposal is,

instead, to use a *detuned two-photon driving*, e.g., of frequency ω_L and amplitude Ω , to squeeze the cavity mode. The driving results in parametric down conversion of mechanical phonons to correlated cavity-photon pairs, which corresponds to the DCE. Furthermore, the SCM frequency completely depends on the detuning $\Delta = \omega_c - \omega_L/2$ and the amplitude Ω . This can be exploited to tune the parametric phonon-photon coupling into resonance, determining a strong amplification of the DCE. When the mechanical mode is driven, e.g., at frequency ω_d and amplitude F , a strong steady-state output-photon flux that is induced by the DCE can be achieved in the laboratory frame. The parametric energy conversion of the mechanical motion to the electromagnetic field, which were predicted in the original DCE proposals, can therefore be observed. The process can be interpreted, in the laboratory frame, as two-photon hyper-Raman scattering [see Fig. 1(b)]. Specifically, in the absence of mechanical excitations, the off-resonant two-photon driving produces only a limited amount of cavity photons, but when mechanical phonons of proper frequency are present, the driving photons are scattered into resonant cavity-photon pairs.

We now analyze the mechanical DCE and its observable signatures in experiments. To begin, we consider the Hamiltonian

$$H = H_{\text{OM}} + H_{\text{CD}} + H_{\text{MD}}. \quad (1)$$

Here, $H_{\text{OM}} = \omega_m b^\dagger b - g_0 a^\dagger a (b + b^\dagger)$ describes a standard optomechanical coupling, $H_{\text{CD}} = \Delta a^\dagger a + \frac{1}{2}\Omega (a^2 + a^{\dagger 2})$ a detuned two-photon cavity driving, and $H_{\text{MD}} = \frac{1}{2}F [\exp(i\omega_d t) b + \exp(-i\omega_d t) b^\dagger]$ a single-phonon mechanical driving. The bare cavity mode a , when parametrically driven, is squeezed with a squeezing parameter $r = \frac{1}{4} \ln [(\Delta + \Omega) / (\Delta - \Omega)]$, and accordingly, is transformed to a squeezed mode a_s , via the Bogoliubov transformation $a_s = \cosh(r)a + \sinh(r)a^\dagger$ [35]. As a result, H_{CD} is diagonalized to $H_{\text{CD}} = \omega_s a_s^\dagger a_s$, where $\omega_s = \sqrt{\Delta^2 - \Omega^2}$ is a controllable SCM frequency. In Fig. 1(c) we plot ω_s as a function of Δ and Ω , and find that the resonance condition $\omega_m = 2\omega_s$, for a parametric coupling between SCM and mechanical mode (see below), can be achieved with experimentally modest parameters. The optomechanical-coupling Hamiltonian is transformed, in terms of a_s , to $H_{\text{OM}} = [-g_{\text{OM}} a_s^\dagger a_s + g_{\text{DCE}} (a_s^2 + a_s^{\dagger 2})] (b + b^\dagger)$, where $g_{\text{OM}} = g_0 \cosh(2r)$ is an effective single-photon optomechanical coupling, and $g_{\text{DCE}} = g_0 \sinh(2r)/2$ is a coupling associated with the DCE. The dynamics under H_{OM} describes a mechanical modulation of the boundary condition of the squeezed field [34, 40, 41], and as $\omega_m \simeq 2\omega_s$, the DCE can be demonstrated in the squeezed frame. Under the rotating-wave approximation, the coherent dynamics of the system is governed by an

effective Hamiltonian,

$$H_{\text{eff}} = \Delta_s a_s^\dagger a_s + \Delta_m b^\dagger b + g_{\text{DCE}} (a_s^2 b^\dagger + \text{H.c.}) + \frac{1}{2} F (b + b^\dagger), \quad (2)$$

where $\Delta_s = \omega_s - \omega_d/2$ and $\Delta_m = \omega_m - \omega_d$. We find that the parametric phonon-photon coupling hybridizes states $|n, k\rangle$ and $|n+2, k-1\rangle$, where n is the SCM photon number and k is the phonon number. For $F = 0$, the unitary evolution under H_{eff} drives the system, for example, from the single-phonon state $|0, 1\rangle$ to the squeezed two-photon state $|2, 0\rangle$. By considering the mechanical and cavity losses, a steady-state SCM photon number is obtained at a nonzero mechanical drive, which produces a steady-state output-photon flux, as discussed below.

To analyze the steady-state behavior, we need to describe the environmental noise. In our approach, we squeeze the a mode to make the effective cavity frequency very close to the mechanical frequency. However, this squeezing also inputs thermal noise and two-photon correlation noise into the cavity. The noise introduced can be filtered out using standard spectroscopic techniques, because its frequency is different from that of the DCE-induced photons. Although these undesired effects do not prevent the DCE observation, they can be suppressed by coupling a squeezed-vacuum bath, e.g., with a squeezing parameter r_e and a reference phase θ_e , to the a mode [42–49]. We assume that $r_e = r$ and $\theta_e = \pm n\pi$ ($n = 1, 3, 5, \dots$), so that the a_s mode is equivalently coupled to a vacuum bath [50]. The full dynamics is therefore determined by the standard master equation

$$\dot{\rho}(t) = i[\rho(t), H_{\text{eff}}] - \frac{\kappa}{2} \mathcal{L}(a_s) \rho(t) - \frac{\gamma_m}{2} \mathcal{L}(b) \rho(t), \quad (3)$$

where κ and γ_m are the cavity and mechanical loss rates, respectively, and we have defined $\mathcal{L}(o)\rho(t) = o^\dagger \rho(t) - 2o\rho(t)o^\dagger + \rho(t)o^\dagger o$. We have also assumed that the mechanical resonator is coupled to a zero-temperature bath (see [50] for an analytical discussion at finite temperatures). The SCM excitation spectrum $\langle a_s^\dagger a_s \rangle_{\text{ss}}(\Delta_s)$, where $\langle o \rangle_{\text{ss}}$ represents a steady-state average value, is plotted in Figs. 2(a) and 2(b). Eliminating the squeezing-induced noise ensures a zero background noise for the excitation spectrum. If the mechanical resonator is driven, then photons are excited from the vacuum, and according to energy conservation, are emitted from the mechanical resonator, together with a resonance peak in the excitation spectrum.

How to observe the DCE.— We now return to the original laboratory frame and consider the steady-state output-photon flux. Because of the squeezing, the steady-state intracavity photon number, $\langle a^\dagger a \rangle_{\text{ss}}$, in the laboratory frame includes two physical contributions, i.e., $\langle a^\dagger a \rangle_{\text{ss}} = \Phi_{\text{BGN}} + \Phi_{\text{DCE}}$, where $\Phi_{\text{BGN}} = \sinh^2(r)$ is the number of background-noise photons contained in

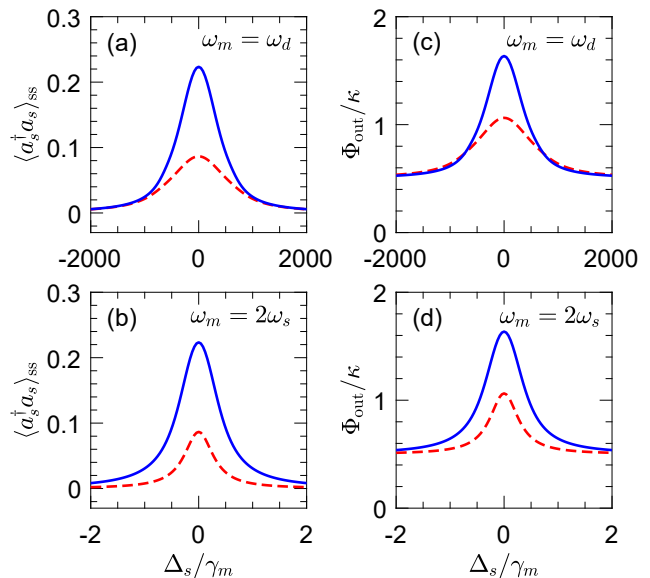


FIG. 2. (a)-(b) Photon number $\langle a_s^\dagger a_s \rangle_{\text{ss}}$ and (c)-(d) photon flux Φ_{out} versus detuning Δ_s . The emergence of the resonance peaks indicates the occurrence of the DCE. We assumed $\omega_m = \omega_d$ in (a) and (c), and $\omega_m = 2\omega_s$ in (b) and (d). Solid curves correspond to $\kappa = 500\gamma_m$ and dashed curves to $\kappa = 1000\gamma_m$. In all plots, we assumed $g_0 = 10\gamma_m$, $F = 15\gamma_m$, $\omega_m = 10^4\gamma_m$, and $\sinh^2(r) = 0.5$.

the squeezed vacuum, and $\Phi_{\text{DCE}} = \langle a_s^\dagger a_s \rangle_{\text{ss}} \cosh(2r) - \text{Re}[\langle a_s^2 \rangle_{\text{ss}}] \sinh(2r)$ is the number of DCE-induced photons. The output-photon flux is then given by $\Phi_{\text{out}} = \kappa(\Phi_{\text{BGN}} + \Phi_{\text{DCE}})$, according to the input-output relation. We plot the flux spectrum $\Phi_{\text{out}}(\Delta_s)$ in Figs. 2(c) and 2(d). There exists a nonzero background noise in the photon flux spectrum, as discussed previously. Nevertheless, when driving the mechanical resonator, the DCE photons are emitted from the cavity, and a resolved resonance peak can be observed. We find that the behavior of the flux spectrum directly reflects that of the excitation spectrum. Hence, the emergence of the resonance peak in the flux spectrum can be considered as an experimentally observable signature of the DCE.

Owing to the existence of the background noise in the flux Φ_{out} , we now discuss the ability to resolve the DCE signal Φ_{DCE} from the background noise Φ_{BGN} at resonance $\omega_m = \omega_d = 2\omega_s$. In order to quantify this, we typically employ the signal-to-noise ratio, defined as $\mathcal{R} = \Phi_{\text{DCE}}/\Phi_{\text{BGN}}$. The signal-resolved regime often requires $\mathcal{R} > 1$, allowing for a resolved DCE-photon detection. We find that, by increasing the mechanical driving F , the signal Φ_{DCE} becomes stronger, but at the same time, the noise Φ_{BGN} remains unchanged. This enables an improvement in the signal-to-noise ratio with the mechanical force. Consequently, the desired signal can be directly driven from the unresolved to resolved regime, as shown in Fig. 3(a). Assuming a realistic

parameter $g_0 = 10\gamma_m$, we find that a mechanical driving of $F = 15\gamma_m$ is able to keep the ratio \mathcal{R} above 1 for $\kappa \leq 1000\gamma_m$. With these parameters, we can obtain $\langle a_s^\dagger a_s \rangle_{ss} \simeq 0.2$, as given in Fig. 2. Therefore, in the laboratory frame, a cavity having a typical linewidth of $\kappa/2\pi = 2.0$ MHz could emit $\simeq 1.4 \times 10^7$ photons per second, which is larger than the background photon emission $\simeq 6.3 \times 10^6$ per second. The ratio \mathcal{R} can be made $\gg 1$ as long as the driving F is further increased, so that the background noise can be even neglected compared to the DCE signal. This is demonstrated in the Supplemental Material [50], where we make a semi-classical approximation for investigating the DCE under a strong- F drive. Note, however, that the signal can still be resolved even for $\mathcal{R} < 1$, if standard techniques of Raman spectroscopy are used. This is because the background noise is due to squeezed photons at frequency $\omega_L/2$, while the DCE photons have a frequency ω_c . The monotonic increase of the flux Φ_{out} at resonance with the driving F can, therefore, be considered as another signature of the mechanical DCE in experiments.

The DCE photons are emitted in pairs, and could exhibit photon bunching [22, 34, 51]. The essential parameter characterizing this property is the equal-time second-order correlation function, $g_s^{(2)}(0) = \langle a_s^{\dagger 2} a_s^2 \rangle_{ss} / \langle a_s^\dagger a_s \rangle_{ss}^2$. We plot it as a function of the mechanical driving in Fig. 3(b). We find that $g_s^{(2)}(0) \simeq 1 / (2 \langle a_s^\dagger a_s \rangle_{ss})$ in the $F \rightarrow 0$ limit, and $\simeq 1$ in the $F \rightarrow \infty$ limit [50]. Hence, for a weak- F drive, the very small $\langle a_s^\dagger a_s \rangle_{ss}$ leads to $g_s^{(2)}(0) \gg 1$. This corresponds to strong photon bunching. Furthermore, we find that with increasing the driving F , the $g_s^{(2)}(0)$ correlation decreases and then, as suggested above, approaches its lower bound equal to 1. These features confirm that the photons are bunched, as required.

In order for the DCE in the squeezed frame to be more directly observed in the laboratory frame, we now consider the limit $\Omega \ll \Delta$. In this limit, the squeezing parameter r is very small and, as a result, the a_s mode can be approximated by the a mode, i.e., $a_s \simeq a$. The effective Hamiltonian becomes $\tilde{H}_{\text{eff}} = \Delta_s a^\dagger a + \Delta_m b^\dagger b + g_{\text{DCE}} (a^2 b^\dagger + \text{H.c.}) + \frac{1}{2} F (b + b^\dagger)$ [50]. The DCE is therefore mapped from the a_s mode onto the a mode, which enables a more direct DCE detection in the laboratory frame. Such a map can be made more accurate by decreasing the ratio Ω/Δ , but at the expense of the DCE radiation strength. Moreover, we also find that the noise induced by squeezing the cavity, which includes thermal noise $\propto \sinh^2(r)$ and two-photon correlation noise $\propto \sinh(2r)$, becomes strongly suppressed, even when there is no squeezed-vacuum bath. Without such a bath, the master equation is the same as given in Eq. (3), but with replacing $a_s \mapsto a$. The observable DCE signatures in the laboratory frame are thus similar to what we have already demonstrated in the

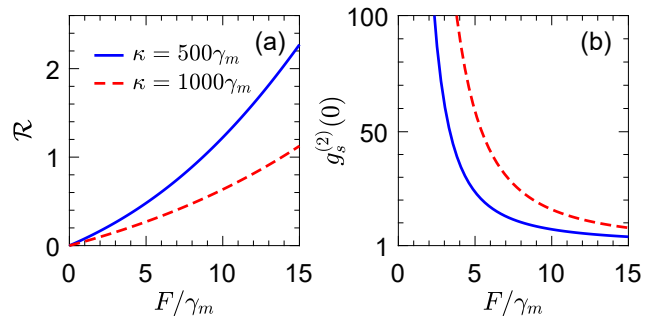


FIG. 3. (a) Signal-to-noise ratio \mathcal{R} and (b) equal-time correlation $g_s^{(2)}(0)$ as a function of the mechanical driving F for $\kappa = 500\gamma_m$ and $1000\gamma_m$. Note that the signal can still be resolved even if $\mathcal{R} < 1$ with standard spectroscopic techniques used, e.g., for Raman signals. The $g_s^{(2)}(0) > 1$ correlation implies that in the squeezed frame, the photons are created in pairs from the quantum vacuum. For both plots, we assumed that $g_0 = 10\gamma_m$, $\omega_m = \omega_d = 2\omega_s$, and $\sinh^2(r) = 0.5$.

squeezed frame for the a_s mode. This map also enables detecting other signatures, e.g., the $g_s^{(2)}(0)$ correlation and the spectrum of emission. For realistic parameters $g_0 = 10\gamma_m$, $F = 15\gamma_m$ and $\Omega/\Delta = 0.1$, we could obtain $\langle a_s^\dagger a_s \rangle_{ss} \simeq 1.8 \times 10^{-3}$ at resonance ($\omega_m = \omega_d = 2\omega_s$) [50]. This results in an output flux $\simeq 2.0 \times 10^4$ photons per second for $\kappa/2\pi = 2$ MHz. This radiation can be measured using single-photon detectors. Here, all the photons radiated from the cavity can be thought of as the DCE signal, because the background noise is $\simeq 0$ in the limit $\Omega \ll \Delta$.

Possible implementations.— As an example, we consider an LC superconducting circuit with a micromechanical membrane (see Ref. [50] for details). In this device, the LC circuit is used to form a single-mode microwave cavity. The mechanical motion of the membrane modulates the capacitance of the LC circuit, and thus the cavity frequency. In order to squeeze the cavity mode, an additional tunable capacitor is embedded into the device. Its cosine-wave modulation serves as a two-photon driving for the cavity mode. The squeezed-vacuum reservoir can be generated through an LC circuit with a tunable capacitor [50], or through a Josephson parametric amplifier [42, 52]. Alternatively, our proposal can be implemented in an optical system such as a whispering-gallery-mode (WGM) microresonator coupled to a mechanical breathing mode [39, 53–58]. The WGM microresonator made from nonlinear crystals exhibits strong optical nonlinearities [59–61], which is the essential requirement for squeezing. The squeezed-vacuum reservoir for the optical cavity can be prepared by pumping a nonlinear medium, e.g., periodically-poled KTiOPO_4 (PPKTP) crystal, in a cavity [62–65].

Conclusions.— We have introduced a method for

how to observe the mechanical DCE in a squeezed optomechanical system. The method eliminates the problematic need for an extremely high mechanical-oscillation frequency and an ultrastrong single-photon optomechanical coupling, and can be applied to a variety of physical systems. Thus, it paves an experimentally feasible path to observing quantum radiation from a moving mirror. Although our proposal involves a two-photon driving, it can still be considered as the DCE in the laboratory frame, because in the absence of mechanical excitations, no photons are emitted at the cavity frequency ω_c . Moreover, even without a squeezed-vacuum bath, all photons emitted at ω_c originate from the parametric conversion of mechanical energy into electromagnetic energy. Such a process can be understood as hyper-Raman scattering [66], either at anti-Stokes (DCE) or Stokes (anti-DCE) frequency. Squeezing the cavity can enable a controllable, ultrastrong light-matter coupling even in optical cavity QED [47, 48], and thus can in principle be applied to implement the observation of the DCE based on a nonadiabatic modulation of this ultrastrong coupling [13–15]. In addition, this squeezing can also enable a virtual-photon-pair mediated coherent coupling, which allows demonstrating the mechanical-energy transfer through the quantum vacuum [41], and simulating nonlinear-optics phenomena with atoms [20, 66, 67]. Finally, we expect that the approach presented here could find diverse applications in theoretical and experimental studies of quantum vacuum radiation.

A.M. and F.N. acknowledge the support of a grant from the John Templeton Foundation. S.S. acknowledges the Army Research Office (ARO) (Proposal No. 73511-PH-RFC). F.N. is supported in part by the: MURI Center for Dynamic Magneto-Optics via the Air Force Office of Scientific Research (AFOSR) (FA9550-14-1-0040), Army Research Office (ARO) (Grant No. Grant No. W911NF-18-1-0358), Asian Office of Aerospace Research and Development (AOARD) (Grant No. FA2386-18-1-4045), Japan Science and Technology Agency (JST) (via the Q-LEAP program, the ImPACT program, and the CREST Grant No. JPMJCR1676), Japan Society for the Promotion of Science (JSPS) (JSPS-RFBR Grant No. 17-52-50023, and JSPS-FWO Grant No. VS.059.18N), and the RIKEN-AIST Challenge Research Fund.

[1] J. Schwinger, “On Gauge Invariance and Vacuum Polarization,” *Phys. Rev.* **82**, 664 (1951).
 [2] S. W. Hawking, “Black hole explosions?” *Nature* **248**, 30 (1974).
 [3] W. G. Unruh, “Notes on black-hole evaporation,” *Phys. Rev. D* **14**, 870 (1976).
 [4] G. T. Moore, “Quantum Theory of the Electromagnetic Field in a Variable-Length One-Dimensional Cavity,” *J.*

Math. Phys. **11**, 2679–2691 (1970).
 [5] S. A. Fulling and P. C. W. Davies, “Radiation from a moving mirror in two dimensional space-time: conformal anomaly,” *Proc. R. Soc. Lond. A* **348**, 393–414 (1976).
 [6] V. V. Dodonov, “Current status of the dynamical Casimir effect,” *Phys. Scr.* **82**, 038105 (2010).
 [7] P. D. Nation, J. R. Johansson, M. P. Blencowe, and F. Nori, “Colloquium: Stimulating uncertainty: Amplifying the quantum vacuum with superconducting circuits,” *Rev. Mod. Phys.* **84**, 1 (2012).
 [8] E. Yablonovitch, “Accelerating reference frame for electromagnetic waves in a rapidly growing plasma: Unruh-Davies-Fulling-Dewitt radiation and the nonadiabatic Casimir effect,” *Phys. Rev. Lett.* **62**, 1742 (1989).
 [9] Y. E. Lozovik, V. G. Tsvetov, and E. A. Vinogradov, “Parametric excitation of vacuum by use of femtosecond laser pulses,” *Phys. Scr.* **52**, 184 (1995).
 [10] M. Croce, D. A. R. Dalvit, F. C. Lombardo, and F. D. Mazzitelli, “Model for resonant photon creation in a cavity with time-dependent conductivity,” *Phys. Rev. A* **70**, 033811 (2004).
 [11] C. Braggio, G. Bressi, G. Carugno, C. Del Noce, G. Galeazzi, A. Lombardi, A. Palmieri, G. Ruoso, and D. Zanello, “A novel experimental approach for the detection of the dynamical Casimir effect,” *Europhys. Lett.* **70**, 754 (2005).
 [12] E. Segev, B. Abdo, O. Shtempluck, E. Buks, and B. Yurke, “Prospects of employing superconducting stripline resonators for studying the dynamical Casimir effect experimentally,” *Phys. Lett. A* **370**, 202–206 (2007).
 [13] C. Ciuti, G. Bastard, and I. Carusotto, “Quantum vacuum properties of the intersubband cavity polariton field,” *Phys. Rev. B* **72**, 115303 (2005).
 [14] S. De Liberato, C. Ciuti, and I. Carusotto, “Quantum Vacuum Radiation Spectra from a Semiconductor Microcavity with a Time-Modulated Vacuum Rabi Frequency,” *Phys. Rev. Lett.* **98**, 103602 (2007).
 [15] S. De Liberato, D. Gerace, I. Carusotto, and C. Ciuti, “Extracavity quantum vacuum radiation from a single qubit,” *Phys. Rev. A* **80**, 053810 (2009).
 [16] L. Garziano, A. Ridolfo, R. Stassi, O. Di Stefano, and S. Savasta, “Switching on and off of ultrastrong light-matter interaction: Photon statistics of quantum vacuum radiation,” *Phys. Rev. A* **88**, 063829 (2013).
 [17] D. Hagenmüller, “All-optical dynamical Casimir effect in a three-dimensional terahertz photonic band gap,” *Phys. Rev. B* **93**, 235309 (2016).
 [18] S. De Liberato, “Virtual photons in the ground state of a dissipative system,” *Nat. Commun.* **8**, 1465 (2017).
 [19] R. de Melo e Souza, F. Impens, and P. A. Maia Neto, “Microscopic dynamical Casimir effect,” *Phys. Rev. A* **97**, 032514 (2018).
 [20] A. F. Kockum, A. Miranowicz, S. De Liberato, S. Savasta, and F. Nori, “Ultrastrong coupling between light and matter,” *Nat. Rev. Phys.* **1**, 19 (2019).
 [21] J. R. Johansson, G. Johansson, C. M. Wilson, and F. Nori, “Dynamical Casimir Effect in a Superconducting Coplanar Waveguide,” *Phys. Rev. Lett.* **103**, 147003 (2009).
 [22] J. R. Johansson, G. Johansson, C. M. Wilson, and F. Nori, “Dynamical Casimir effect in superconducting microwave circuits,” *Phys. Rev. A* **82**, 052509 (2010).
 [23] C. M. Wilson, G. Johansson, A. Pourkabirian,

- M. Simoen, J. R. Johansson, T. Duty, F. Nori, and P. Delsing, "Observation of the dynamical Casimir effect in a superconducting circuit," *Nature (London)* **479**, 376 (2011).
- [24] D. A. R. Dalvit, "Quantum physics: Shaking photons out of the vacuum," *Nature (London)* **479**, 303 (2011).
- [25] J. R. Johansson, G. Johansson, C. M. Wilson, P. Delsing, and F. Nori, "Nonclassical microwave radiation from the dynamical casimir effect," *Phys. Rev. A* **87**, 043804 (2013).
- [26] P. Lähteenmäki, G. S. Paraoanu, J. Hassel, and P. J. Hakonen, "Dynamical Casimir effect in a Josephson metamaterial," *Proc. Natl. Acad. Sci. U. S. A.* **110**, 4234–4238 (2013).
- [27] M. Aspelmeyer, T. J. Kippenberg, and F. Marquardt, "Cavity optomechanics," *Rev. Mod. Phys.* **86**, 1391 (2014).
- [28] A. Lambrecht, M.-T. Jaekel, and S. Reynaud, "Motion Induced Radiation from a Vibrating Cavity," *Phys. Rev. Lett.* **77**, 615 (1996).
- [29] V. V. Dodonov and A. B. Klimov, "Generation and detection of photons in a cavity with a resonantly oscillating boundary," *Phys. Rev. A* **53**, 2664 (1996).
- [30] G. Plunien, R. Schützhold, and G. Soff, "Dynamical Casimir Effect at Finite Temperature," *Phys. Rev. Lett.* **84**, 1882 (2000).
- [31] G. Schaller, R. Schützhold, G. Plunien, and G. Soff, "Dynamical Casimir effect in a leaky cavity at finite temperature," *Phys. Rev. A* **66**, 023812 (2002).
- [32] W.-J. Kim, J. H. Brownell, and R. Onofrio, "Detectability of Dissipative Motion in Quantum Vacuum via Superradiance," *Phys. Rev. Lett.* **96**, 200402 (2006).
- [33] A. S. M. De Castro, A. Cacheffo, and V. V. Dodonov, "Influence of the field-detector coupling strength on the dynamical Casimir effect," *Phys. Rev. A* **87**, 033809 (2013).
- [34] V. Macrì, A. Ridolfo, O. Di Stefano, A. F. Kockum, F. Nori, and S. Savasta, "Nonperturbative Dynamical Casimir Effect in Optomechanical Systems: Vacuum Casimir-Rabi Splittings," *Phys. Rev. X* **8**, 011031 (2018).
- [35] M. O. Scully and M. S. Zubairy, *Quantum Optics* (Cambridge University Press, Cambridge, 1997).
- [36] Z. L. Xiang, S. Ashhab, J. Q. You, and F. Nori, "Hybrid quantum circuits: Superconducting circuits interacting with other quantum systems," *Rev. Mod. Phys.* **85**, 623 (2013).
- [37] X. Gu, A. F. Kockum, A. Miranowicz, Y.-x. Liu, and F. Nori, "Microwave photonics with superconducting quantum circuits," *Phys. Rep.* **718-719**, 1–102 (2017).
- [38] A. Reiserer and G. Rempe, "Cavity-based quantum networks with single atoms and optical photons," *Rev. Mod. Phys.* **87**, 1379 (2015).
- [39] E. Verhagen, S. Deléglise, S. Weis, A. Schliesser, and T. J. Kippenberg, "Quantum-coherent coupling of a mechanical oscillator to an optical cavity mode," *Nature (London)* **482**, 63 (2012).
- [40] C. K. Law, "Interaction between a moving mirror and radiation pressure: A Hamiltonian formulation," *Phys. Rev. A* **51**, 2537 (1995).
- [41] O. Di Stefano, A. Settineri, V. Macrì, A. Ridolfo, R. Stassi, A. F. Kockum, S. Savasta, and F. Nori, "Interaction of Mechanical Oscillators Mediated by the Exchange of Virtual Photon Pairs," *Phys. Rev. Lett.* **112**, 030402 (2019).
- [42] K. W. Murch, S. J. Weber, K. M. Beck, E. Ginossar, and I. Siddiqi, "Reduction of the radiative decay of atomic coherence in squeezed vacuum," *Nature (London)* **499**, 62–65 (2013).
- [43] M. Bartkowiak, L.-A. Wu, and A. Miranowicz, "Quantum circuits for amplification of Kerr nonlinearity via quadrature squeezing," *J. Phys. B* **47**, 145501 (2014).
- [44] X.-Y. Lü, Y. Wu, J. R. Johansson, H. Jing, J. Zhang, and F. Nori, "Squeezed Optomechanics with Phase-Matched Amplification and Dissipation," *Phys. Rev. Lett.* **114**, 093602 (2015).
- [45] J. B. Clark, F. Lecocq, R. W. Simmonds, J. Aumentado, and J. D. Teufel, "Sideband cooling beyond the quantum backaction limit with squeezed light," *Nature (London)* **541**, 191–195 (2017).
- [46] S. Zeytinoglu, A. İmamoglu, and S. Huber, "Engineering Matter Interactions Using Squeezed Vacuum," *Phys. Rev. X* **7**, 021041 (2017).
- [47] W. Qin, A. Miranowicz, P.-B. Li, X.-Y. Lü, J. Q. You, and F. Nori, "Exponentially Enhanced Light-Matter Interaction, Cooperativities, and Steady-State Entanglement Using Parametric Amplification," *Phys. Rev. Lett.* **120**, 093601 (2018).
- [48] C. Leroux, L. C. G. Govia, and A. A. Clerk, "Enhancing Cavity Quantum Electrodynamics via Antisqueezing: Synthetic Ultrastrong Coupling," *Phys. Rev. Lett.* **120**, 093602 (2018).
- [49] H. Vahlbruch, D. Wilken, M. Mehmet, and B. Willke, "Laser Power Stabilization beyond the Shot Noise Limit Using Squeezed Light," *Phys. Rev. Lett.* **121**, 173601 (2018).
- [50] See Supplementary Material, which includes Refs. [68–73], at <http://xxx> for a detailed derivation of the optomechanical master equation, an analytical discussion of the mechanical weak driving at finite temperatures, a semi-classical treatment for the mechanical strong driving, the DCE in the limit $\Omega \ll \Delta$, and a possible implementation with superconducting quantum circuits.
- [51] R. Stassi, A. Ridolfo, O. Di Stefano, M. J. Hartmann, and S. Savasta, "Spontaneous Conversion from Virtual to Real Photons in the Ultrastrong-Coupling Regime," *Phys. Rev. Lett.* **110**, 243601 (2013).
- [52] D. M. Toyli, A. W. Eddins, S. Boutin, S. Puri, D. Hover, V. Bolkhovskiy, W. D. Oliver, A. Blais, and I. Siddiqi, "Resonance Fluorescence from an Artificial Atom in Squeezed Vacuum," *Phys. Rev. X* **6**, 031004 (2016).
- [53] T. J. Kippenberg, H. Rokhsari, T. Carmon, A. Scherer, and K. J. Vahala, "Analysis of Radiation-Pressure Induced Mechanical Oscillation of an Optical Microcavity," *Phys. Rev. Lett.* **95**, 033901 (2005).
- [54] A. Schliesser, P. Del'Haye, N. Nooshi, K. J. Vahala, and T. J. Kippenberg, "Radiation Pressure Cooling of a Micromechanical Oscillator Using Dynamical Backaction," *Phys. Rev. Lett.* **97**, 243905 (2006).
- [55] V. Fiore, Y. Yang, M. C. Kuzyk, R. Barbour, L. Tian, and H. Wang, "Storing Optical Information as a Mechanical Excitation in a Silica Optomechanical Resonator," *Phys. Rev. Lett.* **107**, 133601 (2011).
- [56] C. Dong, V. Fiore, M. C. Kuzyk, and H. Wang, "Optomechanical dark mode," *Science* **338**, 1609–1613 (2012).
- [57] Z. Shen, Y.-L. Zhang, Y. Chen, C.-L. Zou, Y.-F. Xiao, X.-B. Zou, F.-W. Sun, G.-C. Guo, and C.-H. Dong,

- “Experimental realization of optomechanically induced non-reciprocity,” *Nat. Photon.* **10**, 657 (2016).
- [58] F. Monifi, J. Zhang, Ş. K. Özdemir, B. Peng, Y.-x. Liu, F. Bo, F. Nori, and L. Yang, “Optomechanically induced stochastic resonance and chaos transfer between optical fields,” *Nat. Photon.* **10**, 399 (2016).
- [59] J. U. Fürst, D. V. Strekalov, D. Elser, A. Aiello, U. L. Andersen, C. Marquardt, and G. Leuchs, “Quantum Light from a Whispering-Gallery-Mode Disk Resonator,” *Phys. Rev. Lett.* **106**, 113901 (2011).
- [60] F. Sedlmeir, M. R. Foreman, U. Vogl, R. Zeltner, G. Schunk, D. V. Strekalov, C. Marquardt, G. Leuchs, and H. G. L. Schwefel, “Polarization-Selective Out-Coupling of Whispering-Gallery Modes,” *Phys. Rev. Applied* **7**, 024029 (2017).
- [61] L. S. Trainor, F. Sedlmeir, C. Peuntinger, and H. G. L. Schwefel, “Selective Coupling Enhances Harmonic Generation of Whispering-Gallery Modes,” *Phys. Rev. Applied* **9**, 024007 (2018).
- [62] S. Ast, M. Mehmet, and R. Schnabel, “High-bandwidth squeezed light at 1550 nm from a compact monolithic PPKTP cavity,” *Opt. Express* **21**, 13572–13579 (2013).
- [63] T. Serikawa, J. Yoshikawa, K. Makino, and A. Furusawa, “Creation and measurement of broadband squeezed vacuum from a ring optical parametric oscillator,” *Opt. Express* **24**, 28383–28391 (2016).
- [64] H. Vahlbruch, M. Mehmet, K. Danzmann, and R. Schnabel, “Detection of 15 dB Squeezed States of Light and Their Application for the Absolute Calibration of Photoelectric Quantum Efficiency,” *Phys. Rev. Lett.* **117**, 110801 (2016).
- [65] R. Schnabel, “Squeezed states of light and their applications in laser interferometers,” *Phys. Rep.* **684**, 1–51 (2017).
- [66] A. F. Kockum, A. Miranowicz, V. Macrì, S. Savasta, and F. Nori, “Deterministic quantum nonlinear optics with single atoms and virtual photons,” *Phys. Rev. A* **95**, 063849 (2017).
- [67] R. Stassi, V. Macrì, A. F. Kockum, O. Di Stefano, A. Miranowicz, S. Savasta, and F. Nori, “Quantum nonlinear optics without photons,” *Phys. Rev. A* **96**, 023818 (2017).
- [68] M. Lemonde, N. Didier, and A. A. Clerk, “Enhanced nonlinear interactions in quantum optomechanics via mechanical amplification,” *Nat. Commun.* **7** (2016).
- [69] J. R. Johansson, P. D. Nation, and F. Nori, “Qutip: An open-source Python framework for the dynamics of open quantum systems,” *Comput. Phys. Commun.* **183**, 1760–1772 (2012).
- [70] J. R. Johansson, P. D. Nation, and F. Nori, “Qutip 2: A Python framework for the dynamics of open quantum systems,” *Comput. Phys. Commun.* **184**, 1234–1240 (2013).
- [71] S. Butera and I. Carusotto, “Mechanical back-reaction effect of the dynamical Casimir emission,” *arXiv preprint arXiv:1810.11281* (2018).
- [72] D. Sarchi, I. Carusotto, M. Wouters, and V. Savona, “Coherent dynamics and parametric instabilities of microcavity polaritons in double-well systems,” *Phys. Rev. B* **77**, 125324 (2008).
- [73] J. D. Teufel, T. Donner, D. Li, J. W. Harlow, M. S. Allman, K. Cicak, A. J. Sirois, J. D. Whittaker, K. W. Lehnert, and R. W. Simmonds, “Sideband cooling of micromechanical motion to the quantum ground state,” *Nature (London)* **475**, 359 (2011).

SUPPLEMENTAL MATERIAL

This Supplemental Material is organized as follows: In Sec. , we present a detailed derivation of the optomechanical master equation excluding the noise induced by squeezing the cavity mode. An analytical investigation of the dynamical Casimir effect (DCE) at the mechanical weak driving is given in Sec. . In Sec. , a semi-classical approximation is introduced to analyze the DCE, in particular, for the mechanical strong driving. In Sec. , we discuss how to map the DCE from the squeezed frame into the laboratory frame in the limit of $\Omega \ll \Delta$. Finally, in Sec. , we discuss, in detail, an experimentally feasible implementation of our scheme utilizing superconducting quantum circuits.

OPTOMECHANICAL MASTER EQUATION EXCLUDING SQUEEZING-INDUCED NOISES

In order to evaluate the steady-state behavior of the system, its interaction with the environment needs to be described carefully. In our proposal for observing the DCE, we parametrically squeeze the cavity mode. Related methods have been used to enhance the light-matter interaction in optomechanical systems [S1, S2] and in cavity electrodynamics systems [S3, S4]. This can make the squeezed-cavity-mode (SCM) frequency comparable to the mechanical frequency, so that the mechanically induced DCE can be observed in a common optomechanical setup without the need for an ultra-high mechanical frequency and an ultrastrong single-photon optomechanical coupling.

However, the squeezing can also introduce undesired noise, including thermal noise and two-photon correlation, into the cavity. These undesired effects do not prevent the observation of the DCE, because their frequency is different from the DCE signal. Hence, they can be filtered out using standard spectroscopic techniques. We can also remove them by coupling a squeezed-vacuum bath to the bare-cavity mode. In this section, we give a detailed derivation of the master equation when the bare-cavity mode is coupled to a squeezed-vacuum bath and the mechanical mode is coupled to a thermal bath. We show that the noise induced by squeezing the cavity can be completely eliminated.

To begin with, we consider the Hamiltonian for the interaction between the system and the baths, which is given by

$$H_{\text{bath}} = H_{\text{bath}}^0 + H_{\text{bath}}^c + H_{\text{bath}}^m, \quad (\text{S1})$$

where

$$H_{\text{bath}}^0 = \sum_l \nu_l [t_c^\dagger(\nu_l) t_c(\nu_l) + t_m^\dagger(\nu_l) t_m(\nu_l)], \quad (\text{S2})$$

$$H_{\text{bath}}^c = \sum_l \lambda_c(\nu_l) [a^\dagger t_c(\nu_l) + t_c^\dagger(\nu_l) a], \quad (\text{S3})$$

$$H_{\text{bath}}^m = \sum_l \lambda_m(\nu_l) [b^\dagger t_m(\nu_l) + t_m^\dagger(\nu_l) b]. \quad (\text{S4})$$

Here, H_{bath}^0 is the free Hamiltonian of the baths, with $t_{c/m}(\nu_l)$ the annihilation operators for the cavity and mechanical bath modes of frequency ν_l , and $H_{\text{bath}}^{c/m}$ represent the couplings of the cavity and the mechanical resonator to their baths, with the coupling strengths $\lambda_{c/m}(\nu_l)$ depending on the frequency ν_l . To derive the master equation, we first switch into the frame rotating at $H_0 = \omega_L a^\dagger a / 2 + H_{\text{bath}}^0$, to introduce the SCM using the Bogoliubov transformation $a_s = \cosh(r) a + \sinh(r) a^\dagger$. Then, we again switch into the frame rotating at $H_{\text{CD}} = \omega_s a_s^\dagger a_s$, with $\omega_s = \sqrt{\Delta^2 - \Omega^2}$ being the SCM frequency, where $\Delta = \omega_c - \omega_L/2$ is the detuning between the bare-cavity frequency ω_c and the half-frequency, $\omega_L/2$, of the two-photon driving, and Ω is the two-photon driving amplitude. The couplings between the system and the baths are, accordingly, transformed to

$$H_{\text{bath}}^c(t) = a(t) T_c^\dagger(t) + a^\dagger(t) T_c(t), \quad (\text{S5})$$

$$H_{\text{bath}}^m(t) = b(t) T_m^\dagger(t) + b^\dagger(t) T_m(t). \quad (\text{S6})$$

Here, we have defined

$$a(t) = \exp(-i\omega_L t/2) \exp(iH_{\text{CD}}t) a \exp(-iH_{\text{CD}}t), \quad (\text{S7})$$

$$b(t) = \exp(-i\omega_m t) b, \quad (\text{S8})$$

$$T_c(t) = \sum_{\nu_l} \lambda_c(\nu_l) t_c(\nu_l) \exp(-i\nu_l t), \quad (\text{S9})$$

$$T_m(t) = \sum_{\nu_l} \lambda_m(\nu_l) t_m(\nu_l) \exp(-i\nu_l t). \quad (\text{S10})$$

Following the standard procedure in Ref. [S5] and, then, returning to the frame rotating at H_0 , we can obtain the following master equation expressed, in terms of the a_s mode, as

$$\begin{aligned} \frac{d}{dt} \rho(t) &= i[\rho(t), H] \\ &- \frac{\kappa}{2} (N+1) \mathcal{L}(a_s) \rho(t) - \frac{\kappa}{2} N \mathcal{L}(a_s^\dagger) \rho(t) + \frac{\kappa}{2} M \mathcal{L}'(a_s) \rho(t) + \frac{\kappa}{2} M^* \mathcal{L}'(a_s^\dagger) \rho(t) \\ &- \frac{\gamma_m}{2} (n_{\text{th}}+1) \mathcal{L}(b) \rho(t) - \frac{\gamma_m}{2} n_{\text{th}} \mathcal{L}(b^\dagger) \rho(t), \end{aligned} \quad (\text{S11})$$

where the Lindblad superoperators are defined by

$$\mathcal{L}(o) \rho(t) = o^\dagger o \rho(t) - 2o \rho(t) o^\dagger + \rho(t) o^\dagger o, \quad (\text{S12})$$

$$\mathcal{L}'(o) \rho(t) = o o \rho(t) - 2o \rho(t) o + \rho(t) o o, \quad (\text{S13})$$

and N, M are given, respectively, by

$$\begin{aligned} N &= \cosh^2(r) \sinh^2(r_e) + \sinh^2(r) \cosh^2(r_e) \\ &+ \frac{1}{2} \sinh(2r) \sinh(2r_e) \cos(\theta_e), \end{aligned} \quad (\text{S14})$$

$$\begin{aligned} M &= [\sinh(r) \cosh(r_e) + \exp(-i\theta_e) \cosh(r) \sinh(r_e)] \\ &\times [\cosh(r) \cosh(r_e) + \exp(i\theta_e) \sinh(r) \sinh(r_e)], \end{aligned} \quad (\text{S15})$$

corresponding to the thermal noise and two-photon correlation, and where

$$\kappa = 2\pi d_c(\omega_L/2) \lambda_c^2(\omega_L/2), \quad (\text{S16})$$

$$\gamma_m = 2\pi d_m(\omega_m) \lambda_m^2(\omega_m), \quad (\text{S17})$$

represent, respectively, the cavity and mechanical decay rates, with $d_c(\omega_L/2)$ being the density of states for the cavity bath at frequency $\omega_L/2$, and $d_m(\omega_m)$ being the density of states for the mechanical bath at frequency ω_m . Moreover, $n_{\text{th}} = [\exp(\omega_m/k_B T) - 1]^{-1}$ is the equilibrium phonon occupation at temperature T .

Note that, to derive the master equation in Eq. (S11), we have assumed that the central frequency of the squeezed-vacuum bath is equal to half the two-photon driving frequency. In addition, we have made the following approximations,

$$d_c(\omega_L/2 \pm \omega_s) \simeq d_c(\omega_L/2), \quad (\text{S18})$$

$$\lambda_c(\omega_L/2 \pm \omega_s) \simeq \lambda_c(\omega_L/2). \quad (\text{S19})$$

This is because, in our case, the SCM frequency ω_s is tuned to be comparable to the mechanical frequency ω_m (\sim MHz). Thus, it is much smaller than the two-photon driving frequency ω_L (of the order of GHz for microwave light or even THz for optical light).

According to Eqs. (S14) and (S15), we can have $N = M = 0$ for $r_e = r$ and $\theta_e = \pm n\pi$ ($n = 1, 3, 5, \dots$), and thus, we have,

$$\begin{aligned} \frac{d}{dt} \rho(t) &= i[\rho(t), H] - \frac{\kappa}{2} \mathcal{L}(a_s) \rho(t) \\ &- \frac{\gamma_m}{2} (n_{\text{th}}+1) \mathcal{L}(b) \rho(t) - \frac{\gamma_m}{2} n_{\text{th}} \mathcal{L}(b^\dagger) \rho(t). \end{aligned} \quad (\text{S20})$$

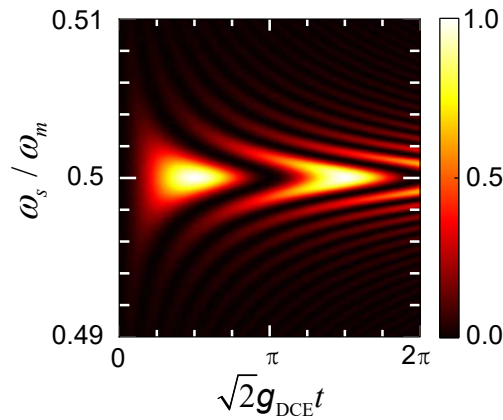


FIG. S1. Parametric energy conversion between the mechanical motion and the squeezed cavity field, obtained from a numerical simulation of Eq. (S21). Under the unitary evolution, one phonon can simultaneously excite two SCM photons. Here, the initial state is $|0, 1\rangle$ and the final state is $|2, 0\rangle$, where the first number in the ket refers to the SCM photon number and the second to the mechanical phonon number, and we set $\omega_m = 10^3 g_0$, $\omega_m = 2\omega_s$, $\Delta = \omega_m$, $F = \gamma_m = \kappa = 0$.

We find from Eq. (S20) that the squeezing-induced noise is completely eliminated, so that the a_s mode is equivalently coupled to the thermal vacuum bath. As we demonstrate below, eliminating this noise can ensure that the background noise is zero for the SCM excitation spectrum in the squeezed frame, and as a result, the background noise of the output-photon flux spectrum in the original laboratory frame only originates from photons contained in the squeezed vacuum. This minimizes the background noise for the observation of the DCE, and thus enables the DCE to be observed more clearly in experiments.

Furthermore, the Hamiltonian in Eqs. (S11) and (S20) is expressed, in terms of the a_s mode, as

$$H = \omega_s a_s^\dagger a_s + \omega_m b^\dagger b - g_{\text{OM}} a_s^\dagger a_s (b + b^\dagger) + g_{\text{DCE}} (a_s^2 + a_s^{\dagger 2}) (b + b^\dagger) + \frac{F}{2} [\exp(i\omega_d t) b + \exp(-i\omega_d t) b^\dagger], \quad (\text{S21})$$

where $g_{\text{OM}} = g_0 \cosh(2r)$ and $g_{\text{DCE}} = g_0 \sinh(2r)/2$, with $r = (1/4) \ln[(\Delta + \Omega)/(\Delta - \Omega)]$ being the squeezing parameter of the cavity. The Hamiltonian H essentially describes the optomechanical system where the boundary condition of a squeezed field is modulated by the mechanical motion of a driven mirror. In the limit $\{\omega_s, \omega_m, \omega_d\} \gg \{g_{\text{OM}}, g_{\text{DCE}}, F\}$, we can apply the rotating-wave approximation, such that the coherent dynamics of the system is governed by the following effective Hamiltonian,

$$H_{\text{eff}} = \Delta_s a_s^\dagger a_s + \Delta_m b^\dagger b + g_{\text{DCE}} (a_s^2 b^\dagger + a_s^{\dagger 2} b) + \frac{F}{2} (b + b^\dagger), \quad (\text{S22})$$

where $\Delta_s = \omega_s - \omega_d/2$ and $\Delta_m = \omega_m - \omega_d$. The master equation in Eq. (S20) is then reduced to

$$\frac{d}{dt} \rho(t) = i[\rho(t), H_{\text{eff}}] - \frac{\kappa}{2} \mathcal{L}(a_s) \rho(t) - \frac{\gamma_m}{2} (n_{\text{th}} + 1) \mathcal{L}(b) \rho(t) - \frac{\gamma_m}{2} n_{\text{th}} \mathcal{L}(b^\dagger) \rho(t). \quad (\text{S23})$$

We find, according to Eq. (S22), that the coupling of the states $|0, 1\rangle$ and $|2, 0\rangle$, where the first number in the ket refers to the SCM photon number and the second one to the mechanical phonon number, is given by

$$g_{|0,1\rangle \leftrightarrow |2,0\rangle} = \sqrt{2} g_{\text{DCE}}. \quad (\text{S24})$$

In the squeezed frame, this means that under the time evolution, one phonon can be converted into two photons, and vice versa, at resonance $\omega_m = 2\omega_s$. To confirm such a state conversion, we perform numerics, as shown in Fig. S1. Specifically, we use the full Hamiltonian H expressed in terms of the a_s mode to calculate the fidelity, $\mathcal{F} = \langle 2, 0 | \exp(-iHt) | 0, 1 \rangle|^2$. It is seen in Fig. S1 that we can have the expected state conversion between light and mechanics, and in particular have a perfect conversion at resonance. Hence, the nonzero mechanical drive can excite the vacuum (or according to energy conservation, the mechanical resonator) to emit a large number of photons. Then, in the presence of the cavity and mechanical loss, this emission can result in a steady-state DCE-induced output-photon flux in the laboratory frame which can be resolved and detected, as discussed in the main article and in the following sections.

DYNAMICAL CASIMIR EFFECT IN THE MECHANICAL WEAK-DRIVING REGIME

In our main article, we have studied the steady-state behavior associated with the DCE, by numerically integrating the master equation in Eq. (S23) [S6, S7]. To study the DCE further, an analytical understanding for the mechanical weak driving is given in this section. Here, we only focus on the resonance situation where $\omega_m = \omega_d = 2\omega_s$.

Let us now derive the steady-state SCM photon number $\langle a_s^\dagger a_s \rangle_{\text{ss}}$, where the subscript ‘‘ss’’ stands for ‘‘steady state’’. To begin, we consider the master equation in Eq. (S23). The involved equations of motion are given, respectively, by

$$\frac{d}{dt} \langle a_s^\dagger a_s \rangle = -4g_{\text{DCE}} \text{Im} [\langle a_s^2 b^\dagger \rangle] - \kappa \langle a_s^\dagger a_s \rangle, \quad (\text{S25})$$

$$\frac{d}{dt} \langle a_s^2 \rangle = -i2g_{\text{DCE}} (2\langle a_s^\dagger a_s b \rangle + \langle b \rangle) - \kappa \langle a_s^2 \rangle, \quad (\text{S26})$$

$$\frac{d}{dt} \langle b \rangle = -i \left(g_{\text{DCE}} \langle a_s^2 \rangle + \frac{F}{2} \right) - \frac{\gamma_m}{2} \langle b \rangle, \quad (\text{S27})$$

$$\frac{d}{dt} \langle b^\dagger b \rangle = 2g_{\text{DCE}} \text{Im} [\langle a_s^2 b^\dagger \rangle] - F \text{Im} [\langle b \rangle] - \gamma_m \langle b^\dagger b \rangle + \gamma_m n_{\text{th}}, \quad (\text{S28})$$

$$\frac{d}{dt} \langle a_s^2 b^\dagger \rangle = i \left(g_{\text{DCE}} \langle a_s^\dagger a_s^2 \rangle - 4g_{\text{DCE}} \langle a_s^\dagger a_s b^\dagger b \rangle + \frac{F}{2} \langle a_s^2 \rangle - 2g_{\text{DCE}} \langle b^\dagger b \rangle \right) - \left(\kappa + \frac{\gamma_m}{2} \right) \langle a_s^2 b^\dagger \rangle, \quad (\text{S29})$$

$$\frac{d}{dt} \langle a_s^\dagger a_s b \rangle = ig_{\text{DCE}} (2\langle a_s^2 b^\dagger b \rangle - \langle a_s^\dagger a_s^3 \rangle - 2\langle a_s^\dagger b^2 \rangle) - i\frac{F}{2} \langle a_s^\dagger a_s \rangle - \left(\kappa + \frac{\gamma_m}{2} \right) \langle a_s^\dagger a_s b \rangle. \quad (\text{S30})$$

Here, $\text{Im}[z]$ represents the imaginary part of z . In fact, owing to the parametric coupling, the Hamiltonian in Eq. (S22) leads to an infinite set of differential equations, which may not be analytically solved. Thus, in order to obtain an analytical result, we neglect the higher-order correlation terms, that is: $\langle a_s^{\dagger 2} a_s^2 \rangle$, $\langle a_s^\dagger a_s b^\dagger b \rangle$, $\langle a_s^2 b^\dagger b \rangle$, $\langle a_s^\dagger a_s^3 \rangle$, and $\langle a_s^{\dagger 2} b^2 \rangle$. This approximation is valid for a weak driving F , as shown below. In such an approximation, the coupled differential equations (S25)–(S30) construct a closed set, so in the steady state we have

$$-4g_{\text{DCE}} \text{Im} [\langle a_s^2 b^\dagger \rangle_{\text{ss}}] - \kappa \langle a_s^\dagger a_s \rangle_{\text{ss}} \simeq 0, \quad (\text{S31})$$

$$-i2g_{\text{DCE}} (2\langle a_s^\dagger a_s \rangle_{\text{ss}} + \langle b \rangle_{\text{ss}}) - \kappa \langle a_s^2 \rangle_{\text{ss}} \simeq 0, \quad (\text{S32})$$

$$-i \left(g_{\text{DCE}} \langle a_s^2 \rangle_{\text{ss}} + \frac{F}{2} \right) - \frac{\gamma_m}{2} \langle b \rangle_{\text{ss}} \simeq 0, \quad (\text{S33})$$

$$2g_{\text{DCE}} \text{Im} [\langle a_s^2 b^\dagger \rangle_{\text{ss}}] - F \text{Im} [\langle b \rangle_{\text{ss}}] - \gamma_m \langle b^\dagger b \rangle_{\text{ss}} + \gamma_m n(\omega_m, T) \simeq 0, \quad (\text{S34})$$

$$i \left(\frac{F}{2} \langle a_s^2 \rangle_{\text{ss}} - 2g_{\text{DCE}} \langle b^\dagger b \rangle_{\text{ss}} \right) - \left(\kappa + \frac{\gamma_m}{2} \right) \langle a_s^2 b^\dagger \rangle_{\text{ss}} \simeq 0, \quad (\text{S35})$$

$$-i\frac{F}{2} \langle a_s^\dagger a_s \rangle_{\text{ss}} - \left(\kappa + \frac{\gamma_m}{2} \right) \langle a_s^\dagger a_s b \rangle_{\text{ss}} \simeq 0. \quad (\text{S36})$$

By solving this closed set of equations, the steady-state SCM photon number is found to be

$$\langle a_s^\dagger a_s \rangle_{\text{ss}} \simeq \frac{4\gamma_m g_{\text{DCE}}^2}{\kappa (2g_{\text{DCE}}^2 + \gamma_0^2)} \left[\frac{\kappa F^2}{2\gamma_m (2g_{\text{DCE}} + \gamma_0^2)} + n_{\text{th}} \right], \quad (\text{S37})$$

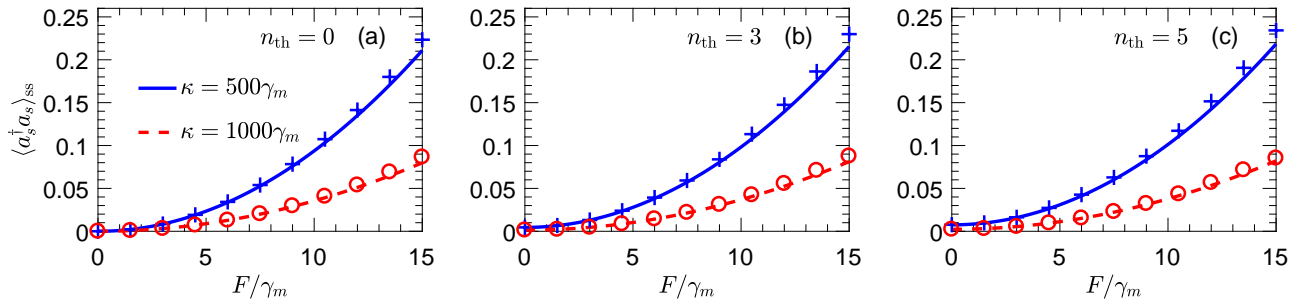


FIG. S2. Photon number $\langle a_s^\dagger a_s \rangle_{\text{ss}}$ versus mechanical driving F for (a) $n_{\text{th}} = 0$, (b) $n_{\text{th}} = 3$, and (c) $n_{\text{th}} = 5$. Curves are analytical results, while symbols are numerical simulations of the master equation in Eq. (S23). Here, we set $g_0 = 10\gamma_m$, $\omega_m = \omega_d = 2\omega_s = 10^4\gamma_m$, and $\Delta = \omega_m$.

where $\gamma_0 = \sqrt{\kappa\gamma_m}/2$. Equation (S37) shows that $\langle a_s^\dagger a_s \rangle_{\text{ss}}$ includes two physical contributions: one from the mechanical driving and the other from the thermal noise. Furthermore, we also find a quadratic increase in $\langle a_s^\dagger a_s \rangle_{\text{ss}}$ with the driving F . To confirm this analytical expression, in Fig. S2 we compare it with exact numerical simulations of the master equation in Eq. (S23). It is seen that the analytical predictions are in good agreement with the exact numerical results, especially for weak F .

According to the Bogoliubov transformation, the steady-state intracavity-photon number $\langle a^\dagger a \rangle_{\text{ss}}$ in the original laboratory frame is expressed as

$$\langle a^\dagger a \rangle_{\text{ss}} = \Phi_{\text{BGN}} + \Phi_{\text{DCE}}. \quad (\text{S38})$$

Here,

$$\Phi_{\text{BGN}} = \sinh^2(r), \quad (\text{S39})$$

is the number of background-noise photons contained in the squeezed vacuum, and

$$\Phi_{\text{DCE}} = \langle a_s^\dagger a_s \rangle_{\text{ss}} \cosh(2r) - \text{Re}[\langle a_s^2 \rangle_{\text{ss}}] \sinh(2r), \quad (\text{S40})$$

is the number of DCE-induced photons. Then, the steady-state output-photon flux is given by

$$\Phi_{\text{out}} = \kappa(\Phi_{\text{BGN}} + \Phi_{\text{DCE}}), \quad (\text{S41})$$

according to the input-output relation $\Phi_{\text{out}} = \kappa\langle a^\dagger a \rangle$. To obtain Φ_{out} analytically, the physical quantities $\langle a_s^\dagger a_s \rangle_{\text{ss}}$ and $\text{Re}[\langle a_s^2 \rangle_{\text{ss}}]$ are involved, as shown in Eq. (S40). The steady-state SCM photon number, $\langle a_s^\dagger a_s \rangle_{\text{ss}}$, is given in Eq. (S37), and further is numerically confirmed in Fig. S2. From the closed set of the steady-state equations given in Eqs. (S31)–(S36), we can straightforwardly find

$$\langle a_s^2 \rangle_{\text{ss}} = -\frac{g_{\text{DCE}}}{2g_{\text{DCE}}^2 + \gamma_0^2} F. \quad (\text{S42})$$

It shows that $|\text{Re}[\langle a_s^2 \rangle_{\text{ss}}]|$ increases linearly with F but is independent of the thermal mechanical noise. This behavior is also numerically confirmed in Fig. S3, showing a good agreement especially for the weak driving F . Note that the derivation of the analytical results and their numerical confirmations originates from neglecting the higher-order correlation terms. In order to exactly describe $\langle a_s^2 \rangle$, such higher-order correlations should be included. By combining Eqs. (S37)–(S42), the steady-state output-photon flux can be analytically expressed as

$$\Phi_{\text{out}} = \frac{4\gamma_m g_{\text{DCE}}^2}{\kappa(2g_{\text{DCE}}^2 + \gamma_0^2)} \left[\frac{\kappa}{2\gamma_m(2g_{\text{DCE}}^2 + \gamma_0^2)} F^2 + n_{\text{th}} \right] \cosh(2r) \quad (\text{S43})$$

$$+ \frac{g_{\text{DCE}}}{2g_{\text{DCE}}^2 + \gamma_0^2} \sinh(2r) F + \kappa \sinh^2(r). \quad (\text{S44})$$

We find from Eq. (S43) that, by increasing the mechanical driving F , the DCE-induced photon flux Φ_{DCE} becomes stronger quadratically, but at the same time, the background-noise photon flux Φ_{BGN} remains unchanged. Therefore, the increase in the total photon flux Φ_{out} with F can be considered as a signature of the mechanical-motion induced DCE.

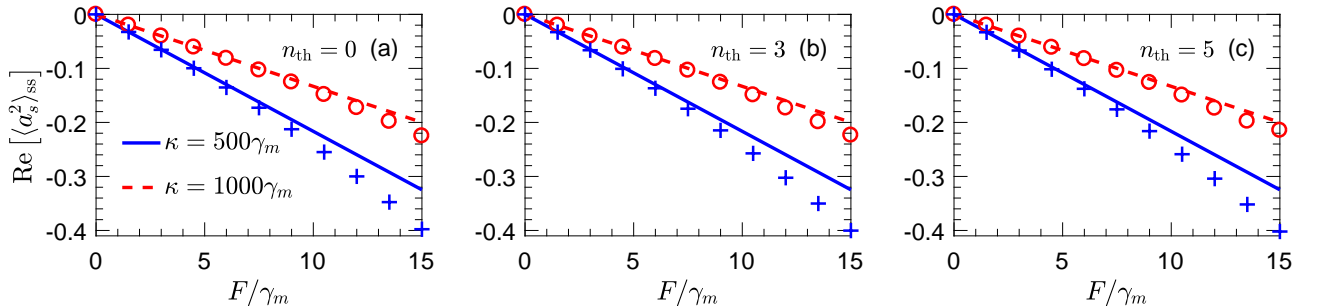


FIG. S3. Real part of the correlation function $\langle a_s^2 \rangle_{\text{ss}}$ versus mechanical driving F for (a) $n_{\text{th}} = 0$, (b) $n_{\text{th}} = 3$, and (c) $n_{\text{th}} = 5$. We assumed the same curve correspondences and the same parameters as in Fig. S2.

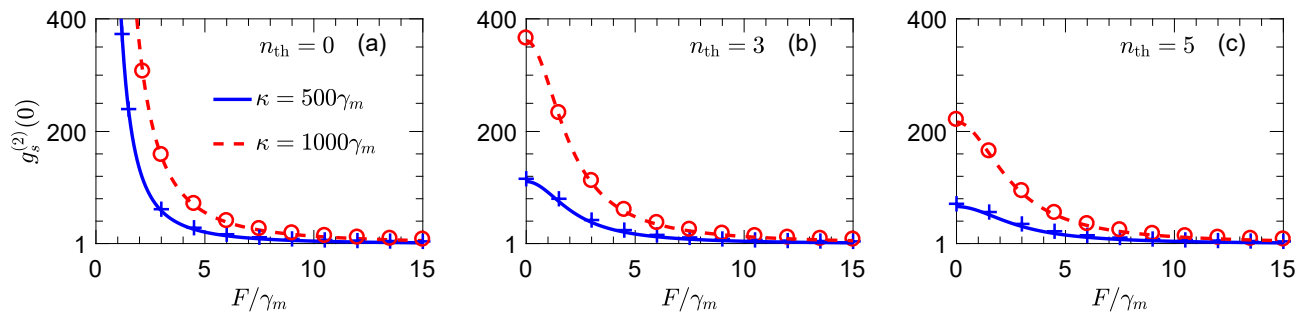


FIG. S4. Correlation function $g_s^{(2)}(0)$ versus mechanical driving F for (a) $n_{\text{th}} = 0$, (b) $n_{\text{th}} = 3$, and (c) $n_{\text{th}} = 5$. We assumed the same curve correspondences and the same parameters as in Fig. S2.

In the DCE process, the photons are emitted in pairs, and therefore, they could exhibit photon bunching [S8–S10]. The essential parameter quantifying this property is the equal-time second-order correlation function, defined as

$$g_s^{(2)}(0) = \frac{\langle a_s^{\dagger 2} a_s^2 \rangle_{\text{ss}}}{\langle a_s^{\dagger} a_s \rangle_{\text{ss}}^2}. \quad (\text{S45})$$

We now derive this second-order correlation function. The equation of motion for $\langle a_s^{\dagger 2} a_s^2 \rangle$ is given by

$$\frac{d}{dt} \langle a_s^{\dagger 2} a_s^2 \rangle = -4g_{\text{DCE}} \{ 2\text{Im} [\langle a_s^{\dagger} a_s^3 b^{\dagger} \rangle] + \text{Im} [\langle a_s^2 b^{\dagger} \rangle] \} - 2\kappa \langle a_s^{\dagger 2} a_s^2 \rangle. \quad (\text{S46})$$

We can neglect the term $\text{Im} [\langle a_s^{\dagger} a_s^3 b^{\dagger} \rangle]$ for the weak driving F . Then, combining Eq. (S31) yields

$$g_s^{(2)}(0) \simeq \frac{1}{2\langle a_s^{\dagger} a_s \rangle_{\text{ss}}}. \quad (\text{S47})$$

In Fig. S4, we plot the $g_s^{(2)}(0)$ correlation as a function of the driving F . In this figure, we compare the analytical and numerical results, and show an exact agreement. Owing to a very small of $\langle a_s^{\dagger} a_s \rangle_{\text{ss}}$ for the mechanical weak driving, $g_s^{(2)}(0)$ is very large as shown in Fig. S4, which corresponds to large photon bunching. With increasing the driving F , we also find that the $g_s^{(2)}(0)$ correlation decreases, and as demonstrated more explicitly in the Sec. , it would approach a lower bound equal to 1, thereby implying that the DCE radiation field becomes a coherent state in the limit of the mechanical strong driving, $F \rightarrow \infty$.

SEMI-CLASSICAL TREATMENT FOR THE DYNAMICAL CASIMIR EFFECT

In Sec. we have analytically discussed the DCE process when the mechanical driving F is weak. There, the higher-order correlations that arise from the parametric coupling are neglected, and the resulting expressions can predict the system behavior well. For strong- F driving, all high-order correlations should be included to exactly describe the system; but in this case, finding solutions analytically or even numerically becomes much more difficult. In order to investigate the DCE in the strong- F regime, in this section we employ a semi-classical treatment [S11]. For simplicity, but without loss of generality, here we assume that the mechanical resonator is coupled to a zero-temperature bath. For finite temperatures, the discussion below is still valid, as long as the total number of phonons is much larger than the number of thermal phonons.

Excitation spectrum and output-photon flux spectrum in the steady state

We again begin with the master equation in Eq. (S23) and, accordingly, obtain

$$\frac{d}{dt} \langle a_s^\dagger a_s \rangle = -4g_{\text{DCE}} \text{Im} [\langle a_s^2 \rangle \langle b \rangle^*] - \kappa \langle a_s^\dagger a_s \rangle, \quad (\text{S48})$$

$$\frac{d}{dt} \langle a_s^2 \rangle = -i2\Delta_s \langle a_s^2 \rangle - i2g_{\text{DCE}} (2\langle a_s^\dagger a_s \rangle + 1) \langle b \rangle - \kappa \langle a_s^2 \rangle, \quad (\text{S49})$$

$$\frac{d}{dt} \langle b \rangle = -i \left(\Delta_m \langle b \rangle + g_{\text{DCE}} \langle a_s^2 \rangle + \frac{F}{2} \right) - \frac{\gamma_m}{2} \langle b \rangle. \quad (\text{S50})$$

Here, we have made the semiclassical approximation, such that $\langle a_s^2 b^\dagger \rangle \simeq \langle a_s^2 \rangle \langle b \rangle^*$ and $\langle a_s^\dagger a_s b \rangle \simeq \langle a_s^\dagger a_s \rangle \langle b \rangle$. Under this approximation, the fluctuation correlation between the cavity and the mechanical resonator is neglected. It is found that Eqs. (S48)–(S50) construct a closed set.

excitation spectrum for resonant mechanical driving: $\omega_m = \omega_d$

We first consider the case of a resonant mechanical driving (i.e., $\omega_m = \omega_d$). In this case, we have $\Delta_m = 0$, and the steady-state SCM photon number $\langle a_s^\dagger a_s \rangle_{\text{ss}}$ satisfies a cubic equation,

$$g_{\text{DCE}}^4 x^3 - g_{\text{DCE}}^2 (g_{\text{DCE}}^2 - \gamma_0^2) x^2 + \left[\frac{1}{4} (\Delta_s^2 \gamma_m^2 + \gamma_0^4) - g_{\text{DCE}}^2 (F^2 + \gamma_0^2) \right] x - \frac{1}{4} (\Delta_s^2 \gamma_m^2 + \gamma_0^4) = 0, \quad (\text{S51})$$

where $\gamma_0 = \sqrt{\kappa \gamma_m / 2}$ and $x = 2\langle a_s^\dagger a_s \rangle_{\text{ss}} + 1$. The solutions of such a equation can be exactly obtained using the Cardano formula. Then, the steady-state $\langle a_s^2 \rangle$ and $\langle b \rangle$ are given, respectively, by

$$\langle a_s^2 \rangle_{\text{ss}} = -\frac{g_{\text{DCE}}}{2g_{\text{DCE}}^2 x + \gamma_0^2 + i\Delta_s \gamma_m} F x, \quad (\text{S52})$$

$$\langle b \rangle_{\text{ss}} = -\frac{(-2\Delta_s + i\kappa)}{2g_{\text{DCE}}^2 x + \gamma_0^2 + i\Delta_s \gamma_m} \frac{F}{2}. \quad (\text{S53})$$

For simplicity, we numerically solve the cubic equation (S51), and in Fig. S5 we plot $\langle a_s^\dagger a_s \rangle_{\text{ss}}$, $\text{Re} [\langle a_s^2 \rangle_{\text{ss}}]$, and $|\langle b \rangle_{\text{ss}}|^2$ versus the detuning Δ_s for $\kappa = 500\gamma_m$ and $1000\gamma_m$. At large detunings, the resonantly driven mechanical resonator is effectively decoupled from the cavity mode. As a consequence, there is almost no conversion of mechanical energy into photons. Thus at large detunings, the mechanical phonon number $|\langle b \rangle_{\text{ss}}|^2$ quickly approaches $(F/\gamma_m)^2$, i.e., the steady-state phonon number when the mechanical resonator is completely uncoupled. Meanwhile, both photon

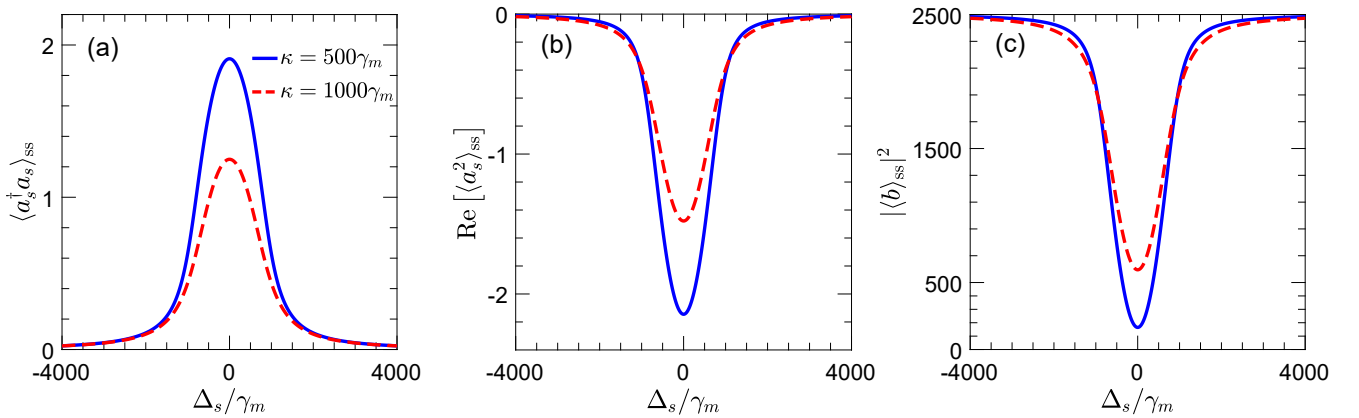


FIG. S5. (a) Photon number $\langle a_s^\dagger a_s \rangle_{\text{ss}}$, (b) real part of the correlation function $\langle a_s^2 \rangle_{\text{ss}}$, and (c) phonon number $|\langle b \rangle_{\text{ss}}|^2$ versus detuning $\Delta_s = \omega_s - \omega_d/2$ for $\kappa = 500\gamma_m$ (solid curves) and $\kappa = 1000\gamma_m$ (dashed curves). We have assumed that $\omega_m = \omega_d$, $g_0 = 10\gamma_m$, $F = 50\gamma_m$, and $\sinh^2(r) = 0.5$.

number $\langle a_s^\dagger a_s \rangle_{\text{ss}}$ and correlation function $\langle a_s^2 \rangle_{\text{ss}}$ are very close to zero. As the detuning decreases, the effective parametric coupling between the mechanical motion and the cavity mode increases, and the parametric conversion from mechanical energy into photons is accordingly enhanced. Such an energy conversion is maximized at resonance $\omega_m = \omega_d = 2\omega_s$. Thus, when decreasing the detuning, both $\langle a_s^\dagger a_s \rangle_{\text{ss}}$ and $|\text{Re}[\langle a_s^2 \rangle_{\text{ss}}]|$ increase but $|\langle b \rangle_{\text{ss}}|^2$ decreases, as shown in Fig. S5. In particular, $\langle a_s^\dagger a_s \rangle_{\text{ss}}$ and $|\text{Re}[\langle a_s^2 \rangle_{\text{ss}}]|$ reach their maximum values at resonance, and at the same time, $|\langle b \rangle_{\text{ss}}|^2$ reaches its minimum value. This behavior implies that the photons are emitted by the mechanical resonator.

excitation spectrum for resonant parametric coupling: $\omega_m = 2\omega_s$

We next consider the case of a resonant parametric coupling (i.e., $\omega_m = 2\omega_s$). In this case, we have $\Delta_m = 2\Delta_s = \Delta$, and the steady-state $\langle a_s^\dagger a_s \rangle$ also satisfies a cubic equation

$$g_{\text{DCE}}^4 x^3 - g_{\text{DCE}}^2 (g_{\text{DCE}}^2 + \Delta^2 - \gamma_0^2) x^2 + \left\{ \frac{1}{4} [(\Delta^2 - \gamma_0^2)^2 + \Delta^2 \gamma_1^2] + g_{\text{DCE}}^2 (\Delta^2 - \gamma_0^2 - F^2) \right\} x - \frac{1}{4} [(\Delta^2 - \gamma_0^2)^2 + \Delta^2 \gamma_1^2] = 0, \quad (\text{S54})$$

where $\gamma_1 = \kappa + \gamma_m/2$. This cubic equation can also be exactly solved using the Cardano formula, and then the steady-state $\langle a_s^2 \rangle$ and $\langle b \rangle$ are given, respectively, by

$$\langle a_s^2 \rangle_{\text{ss}} = -\frac{g_{\text{DCE}}}{2g_{\text{DCE}} x - \Delta^2 + \gamma_0^2 + i\Delta\gamma_1} Fx, \quad (\text{S55})$$

$$\langle b \rangle_{\text{ss}} = -\frac{(-\Delta + i\kappa)}{2g_{\text{DCE}} x - \Delta^2 + \gamma_0^2 + i\Delta\gamma_1} \frac{F}{2}. \quad (\text{S56})$$

We numerically solve the cubic equation (S54), and in Fig. S6, we plot $\langle a_s^\dagger a_s \rangle_{\text{ss}}$, $\text{Re}[\langle a_s^2 \rangle_{\text{ss}}]$, and $|\langle b \rangle_{\text{ss}}|^2$ versus the detuning Δ_s for $\kappa = 500\gamma_m$ and $1000\gamma_m$. At large detunings, the mechanical driving is effectively decoupled from the mechanical resonator, so that almost no phonons are excited and almost no photons are emitted. As the detuning decreases, the mechanical phonon number increases, which strengthens the parametric conversion from mechanical energy into photons, and in turn, leads to an increase in the excited photon number. This process is maximized at resonance $\omega_m = \omega_d = 2\omega_s$. Thus, we find, as shown in Fig. S6, that with decreasing the detuning, not only $\langle a_s^\dagger a_s \rangle_{\text{ss}}$ and $|\text{Re}[\langle a_s^2 \rangle_{\text{ss}}]|$ but also $|\langle b \rangle_{\text{ss}}|^2$ increases, and that they simultaneously reach their maximum values at resonance. This behavior also implies that the photons are emitted by the mechanical resonator.

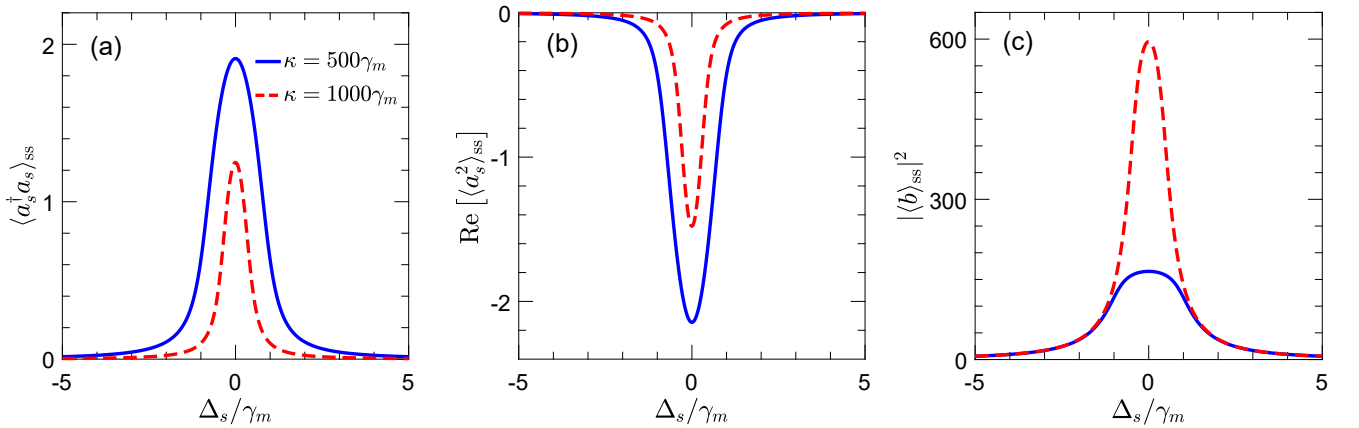


FIG. S6. (a) Photon number $\langle a_s^\dagger a_s \rangle_{\text{ss}}$, (b) real part of the correlation function $\langle a_s^2 \rangle_{\text{ss}}$, and (c) phonon number $|\langle b \rangle_{\text{ss}}|^2$ versus detuning $\Delta_s = \omega_s - \omega_d/2$ for $\kappa = 500\gamma_m$ (solid curves) and $\kappa = 1000\gamma_m$ (dashed curves). We have assumed that $\omega_m = 2\omega_s$, $g_0 = 10\gamma_m$, $F = 50\gamma_m$, and $\sinh^2(r) = 0.5$.

Having obtained $\langle a_s^\dagger a_s \rangle_{ss}$ and $\langle a_s^2 \rangle_{ss}$ in the squeezed frame, we can, according to the Bogoliubov transformation, calculate the steady-state intracavity photon number $\langle a^\dagger a \rangle_{ss}$ in the original laboratory frame, as given in Eq. (S38). Then we can calculate the steady-state output-photon flux Φ_{out} according to the input-output relation, given in Eq. (S41). We plot the photon flux Φ_{out} as a function of the detuning Δ_s in Fig. S7. As expected, for a given mechanical driving, we can observe a resonance peak, corresponding to the maximum value of the photon flux. This behavior in the laboratory frame can directly reflect the behavior of the excitation spectrum $\langle a_s^\dagger a_s \rangle_{ss}(\Delta_s)$ in the squeezed frame in Figs. S5(a) and S6(a). This is because the background noise Φ_{BGN} remains unchanged when the detuning is changed, and the peak completely arises from the DCE in the squeezed frame. Thus, the appearance of the peak of the output flux spectrum $\Phi_{\text{out}}(\Delta_s)$ can be considered as an experimentally observable signature of the DCE.

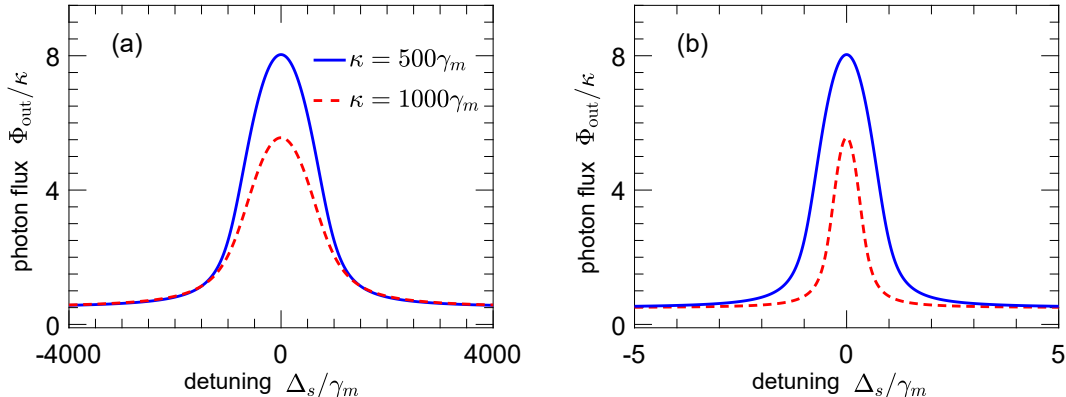


FIG. S7. Steady-state output-photon flux Φ_{out} as a function of the detuning $\Delta_s = \omega_s - \omega_d/2$ for $\kappa = 500\gamma_m$ (solid curves) and $1000\gamma_m$ (dashed curves). We assumed that $\omega_m = \omega_d$ (resonant mechanical driving) in (a) and $\omega_m = 2\omega_s$ (resonant parametric coupling) in (b). For both plots, we assumed that $g_0 = 10\gamma_m$, $F = 50\gamma_m$, and $\sinh^2(r) = 0.5$.

Signal-to-noise ratio and second-order correlation function at resonance

As mentioned before, there exists a background noise Φ_{BGN} in the flux Φ_{out} . Thus, we need to analyze the ability of our proposal to resolve the DCE-induced signal from the background noise. To quantitatively describe this ability, we typically employ the signal-to-noise ratio defined as

$$\mathcal{R} = \frac{\Phi_{\text{DCE}}}{\Phi_{\text{BGN}}}. \quad (\text{S57})$$

Without loss of generality, we only focus on the ratio \mathcal{R} at resonance $\omega_m = \omega_d = 2\omega_s$. Under this resonance condition, the cubic equation satisfied by $\langle a_s^\dagger a_s \rangle_{ss}$ becomes

$$g_{\text{DCE}}^4 x^3 - g_{\text{DCE}}^2 (g_{\text{DCE}}^2 - \gamma_0^2) x^2 + \left[\frac{\gamma_0^4}{4} - g_{\text{DCE}}^2 (\gamma_0^2 + F^2) \right] x - \frac{\gamma_0^4}{4} = 0, \quad (\text{S58})$$

where $x = 2\langle a_s^\dagger a_s \rangle_{ss} + 1$. Then, $\langle a_s^2 \rangle_{ss}$ and $\langle b \rangle_{ss}$ are given by

$$\langle a_s^2 \rangle_{ss} = -\frac{g_{\text{DCE}}}{2g_{\text{DCE}}^2 x + \gamma_0^2} F x, \quad (\text{S59})$$

$$\langle b \rangle_{ss} = -\frac{i\kappa}{2g_{\text{DCE}}^2 x + \gamma_0^2} \frac{F}{2}. \quad (\text{S60})$$

We plot the ratio \mathcal{R} versus the driving F in Fig. S8(a). We find that the signal-to-noise ratio monotonically increases with the mechanical driving. This is owing to the fact that an increase in the mechanical driving leads to an increase in the number of DCE-induced photons, but at the same time leaves the number of background-noise photons unchanged.

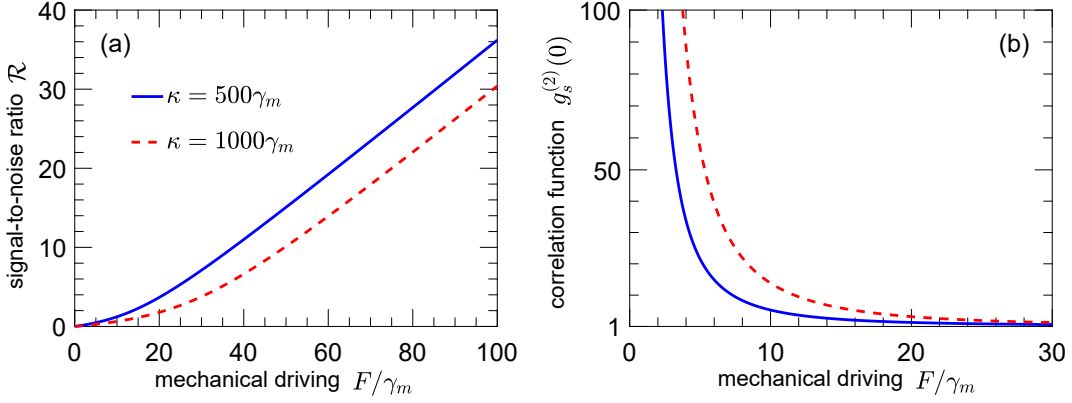


FIG. S8. (a) Signal-to-noise ratio \mathcal{R} and (b) correlation function $g_s^{(2)}(0)$ versus the mechanical driving F for $\kappa = 500\gamma_m$ (solid curves) and $1000\gamma_m$ (dashed curves). For both plots, we assumed that $\omega_m = \omega_d = 2\omega_s$, $g_0 = 10\gamma_m$, and $\sinh^2(r) = 0.5$.

For modest parameters of $F = 100\gamma_m$, we find that the ratio \mathcal{R} can be made larger than 30 for $\kappa \leq 1000\gamma_m$. In this case, the background noise can be ignored compared to the DCE signal. Note that the ratio \mathcal{R} can further increase, as long as the mechanical driving further increases.

The equal-time second-order correlation function is defined in Eq. (S45). Similarly to the discussion of the signal-to-noise ratio \mathcal{R} , we also only focus on the $g_s^{(2)}(0)$ correlation at resonance $\omega_m = \omega_d = 2\omega_s$. In the semi-classical treatment presented in this section, $\langle a_s^{\dagger 2} a_s^2 \rangle_{\text{ss}}$ can be approximated as $\langle a_s^{\dagger 2} a_s^2 \rangle_{\text{ss}} \simeq |\langle a_s^2 \rangle_{\text{ss}}|^2$, and as a result, the $g_s^{(2)}(0)$ correlation is reduced to

$$g_s^{(2)}(0) \simeq \frac{|\langle a_s^2 \rangle_{\text{ss}}|^2}{\langle a_s^{\dagger} a_s \rangle_{\text{ss}}^2}, \quad (\text{S61})$$

which is plotted as a function of the mechanical driving in Fig. S8(b). We find that $g_s^{(2)}(0)$ starts with very large values, and as the mechanical driving increases, $g_s^{(2)}(0)$ then decreases approaching 1. This behavior, as expected, suggests the phenomenon of photon bunching, thus confirming the DCE.

Analytical solutions in the limits $F \rightarrow 0$ and $F \rightarrow \infty$

In order to have a better analytical understanding, let us now consider the limit of $F \rightarrow 0$ and the opposite limit of $F \rightarrow \infty$, at resonance $\omega_m = \omega_d = 2\omega_s$. For the former limit, we have $\langle a_s^{\dagger} a_s \rangle_{\text{ss}} \rightarrow 0$, and thus, $x^n \simeq 1 + 2n\langle a_s^{\dagger} a_s \rangle$ for $n = 0, 1, 2, \dots$. Based on this, an approximate solution of the cubic equation in Eq. (S58) is found to be

$$\langle a_s^{\dagger} a_s \rangle_{\text{ss}} \simeq \frac{2g_{\text{DCE}}^2}{(2g_{\text{DCE}}^2 + \gamma_0^2)} F^2, \quad \text{when } F \rightarrow 0, \quad (\text{S62})$$

which corresponds to Eq. (S37) for $n_{\text{th}} = 0$. Analogously, we obtain

$$\langle a_s^2 \rangle_{\text{ss}} \simeq -\frac{g_{\text{DCE}}}{2g_{\text{DCE}}^2 + \gamma_0^2} F, \quad \text{when } F \rightarrow 0, \quad (\text{S63})$$

$$\langle b \rangle_{\text{ss}} \simeq -\frac{i\kappa}{2g_{\text{DCE}}^2 + \gamma_0^2} \frac{F}{2}, \quad \text{when } F \rightarrow 0. \quad (\text{S64})$$

Note that Eq. (S63) corresponds to Eq. (S42). Therefore, according to Eq. (S43), we obtain a quadratic increase in the ratio $\mathcal{R} = \Phi_{\text{DCE}}/\Phi_{\text{BGN}} \propto F$ with large driving F , as shown in Fig. S8(a). In the opposite limit of $F \rightarrow \infty$, we

have $x \rightarrow 2\langle a_s^\dagger a_s \rangle_{\text{ss}}$, and then obtain

$$\langle a_s^\dagger a_s \rangle_{\text{ss}} \simeq \frac{F}{2g_{\text{DCE}}}, \quad \text{when } F \rightarrow \infty, \quad (\text{S65})$$

$$\langle a_s^2 \rangle_{\text{ss}} \simeq -\frac{F}{2g_{\text{DCE}}}, \quad \text{when } F \rightarrow \infty, \quad (\text{S66})$$

$$\langle b \rangle_{\text{ss}} \simeq -\frac{i\kappa}{4g_{\text{DCE}}}, \quad \text{when } F \rightarrow \infty. \quad (\text{S67})$$

Consequently, the photon flux Φ_{out} is given by

$$\Phi_{\text{DCE}} = \frac{F}{2g_{\text{DCE}}} \exp(2r), \quad \text{when } F \rightarrow \infty. \quad (\text{S68})$$

This indicates a linear increase in the ratio \mathcal{R} with the driving F , as shown in Fig. S8(a).

For the $g_s^{(2)}(0)$ correlation in the limit of $F \rightarrow 0$, we find

$$g_s^{(2)}(0) \simeq \frac{1}{2\langle a_s^\dagger a_s \rangle_{\text{ss}}}, \quad \text{when } F \rightarrow 0, \quad (\text{S69})$$

which is the same as Eq. (S47). This corresponds to a large $g_s^{(2)}(0)$ as in Fig. S8(b) and, thus, to large photon bunching. Furthermore, in the opposite limit of $F \rightarrow \infty$, the correlation function $g_s^{(2)}(0)$ is approximately equal to 1, i.e.,

$$g_s^{(2)}(0) \simeq 1, \quad \text{when } F \rightarrow \infty, \quad (\text{S70})$$

as shown Fig. S8(b). This means that the DCE radiation field is approximately in a coherent state.

Stability analysis

We now turn to multistability effects of our system. As discussed previously, in the semi-classical approximation, the system is governed by a cubic function. However, a cubic function has three solutions, and thus the system may exhibit multistability effects. To analyze them, we need to perform steady-state analysis [S12]. Thus, we express the quantities $\langle a_s^\dagger a_s \rangle$, $\langle a_s^2 \rangle$, and $\langle b \rangle$ as the sum of their steady-state values ($\langle a_s^\dagger a_s \rangle_{\text{ss}}$, $\langle a_s^2 \rangle_{\text{ss}}$, $\langle b \rangle_{\text{ss}}$) and time-dependent small perturbations [$\delta_1(t)$, $\delta_2(t)$, $\delta_3(t)$], that is,

$$\langle a_s^\dagger a_s \rangle = \langle a_s^\dagger a_s \rangle_{\text{ss}} + \delta_1(t), \quad (\text{S71})$$

$$\langle a_s^2 \rangle = \langle a_s^2 \rangle_{\text{ss}} + \delta_2(t), \quad (\text{S72})$$

$$\langle b \rangle = \langle b \rangle_{\text{ss}} + \delta_3(t). \quad (\text{S73})$$

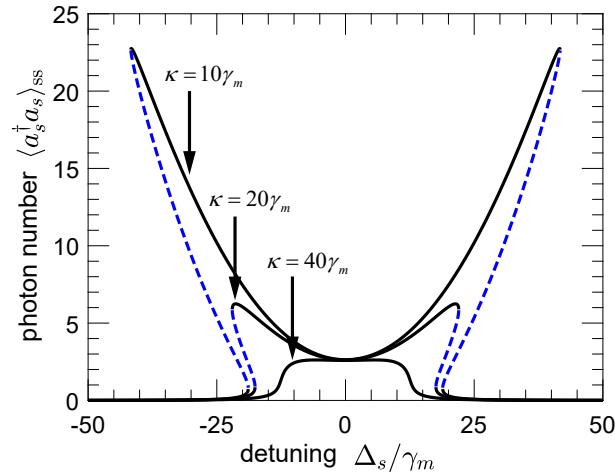


FIG. S9. Steady-state SCM photon number $\langle a_s^\dagger a_s \rangle_{\text{ss}}$ as a function of the detuning Δ_s for $\kappa = 10\gamma_m$, $20\gamma_m$, and $40\gamma_m$. Dashed curves represent unstable solutions. Here, we assumed that $\omega_m = 2\omega_s$, $g_0 = 10\gamma_m$, $F = 50\gamma_m$, and $\sinh^2(r) = 0.5$.

Then, substituting these equations into Eqs. (S48), (S49), and (S50) yields

$$\frac{d}{dt}\delta_1(t) = i2g_{\text{DCE}}(\langle b \rangle_{\text{ss}}^* \delta_2 + \langle a_s^2 \rangle_{\text{ss}} \delta_3^* - \langle b \rangle_{\text{ss}} \delta_2^* - \langle a_s^2 \rangle_{\text{ss}}^* \delta_3) - \kappa \delta_1, \quad (\text{S74})$$

$$\frac{d}{dt}\delta_2(t) = -i2\Delta_s \delta_2 - i2g_{\text{DCE}}(2\langle a_s^\dagger a_s \rangle_{\text{ss}} + 1) \delta_3 - i4g_{\text{DCE}} \delta_1 \langle b \rangle_{\text{ss}} - \kappa \delta_2, \quad (\text{S75})$$

$$\frac{d}{dt}\delta_3(t) = -i\Delta_m \delta_3 - ig_{\text{DCE}} \delta_2 - \frac{\gamma_m}{2} \delta_3. \quad (\text{S76})$$

We further make the following replacements,

$$\delta_1(t) \mapsto \exp(-i\omega t) x_1 + \exp(i\omega^* t) y_1^*, \quad (\text{S77})$$

$$\delta_2(t) \mapsto \exp(-i\omega t) x_2 + \exp(i\omega^* t) y_2^*, \quad (\text{S78})$$

$$\delta_3(t) \mapsto \exp(-i\omega t) x_3 + \exp(i\omega^* t) y_3^*, \quad (\text{S79})$$

where x_k and y_k ($k = 1, 2, 3$) are time-independent complex numbers, and ω denotes a complex frequency. Then, the coupled equations (S74), (S75), and (S76) can be rewritten as

$$M\Psi = \omega\Psi, \quad (\text{S80})$$

where

$$\Psi = (x_1, y_1, x_2, y_2, x_3, y_3)^T, \quad (\text{S81})$$

$$M = i \begin{pmatrix} -\kappa & 0 & A^* & A & B^* & B \\ 0 & -\kappa & A^* & A & B^* & B \\ 2A & 0 & -i2\Delta_s - \kappa & 0 & C & 0 \\ 0 & 2A^* & 0 & i2\Delta_s - \kappa & 0 & C^* \\ 0 & 0 & -ig_{\text{DCE}} & 0 & -i\Delta_m - \gamma_m/2 & 0 \\ 0 & 0 & 0 & ig_{\text{DCE}} & 0 & i\Delta_m - \gamma_m/2 \end{pmatrix}, \quad (\text{S82})$$

where $A = -i2g_{\text{DCE}}\langle b \rangle_{\text{ss}}$, $B = i2g_{\text{DCE}}\langle a_s^2 \rangle_{\text{ss}}$, and $C = -i2g_{\text{DCE}}(2\langle a_s^\dagger a_s \rangle_{\text{ss}} + 1)$. If all imaginary parts of the eigenvalues of the matrix M are negative, then the system is stable; otherwise the system is unstable [S13]. According to this criterion, we estimate the stability of our system. We find that for the parameters used in the above discussion about the DCE, the system does not exhibit multistability. Furthermore, when the mechanical loss is close to the cavity loss, we find for $\omega_m = 2\omega_s$ that the system becomes multistable, as shown in Fig. S9.

MAPPING THE DYNAMICAL CASIMIR EFFECT FROM THE SQUEEZED INTO LABORATORY FRAME IN THE LIMIT $\Omega/\Delta \ll 1$

The DCE considered in this work occurs in the squeezed frame. To observe it in the laboratory frame, we can, according to the Bogoliubov transformation $a_s = \cosh(r)a + \sinh(r)a^\dagger$, convert quantum phenomena associated with the DCE from the squeezed frame into the laboratory frame. Based on this, we have introduced two characteristic signatures in the output-photon flux spectrum, including the emergence of a resolved resonance peak and the monotonic increase in the maximum value of this peak with a mechanical driving, as mentioned in the above sections and also in the main article. To enable the DCE in the squeezed frame to be more directly observed in the laboratory frame, we now consider the limit $\Omega \ll \Delta$. In this limit, we can find that the a_s mode becomes well approximated by the a mode, so that the DCE can be directly mapped into the laboratory frame. Meanwhile, we also find that the noise induced by squeezing the cavity becomes strongly suppressed, even when there is no squeezed-vacuum bath. Therefore, in this section, we focus on the case where such a squeezed-vacuum bath is absent.

The master equation determining the full dynamics of the system in the absence of the squeezed-vacuum bath (i.e., $r_e = 0$) is given by,

$$\begin{aligned} \frac{d}{dt}\rho(t) = & i[\rho(t), H_{\text{eff}}] - \frac{\kappa}{2}\mathcal{L}(a)\rho(t) \\ & - \frac{\gamma_m}{2}(n_{\text{th}} + 1)\mathcal{L}(b)\rho(t) - \frac{\gamma_m}{2}n_{\text{th}}\mathcal{L}(b^\dagger)\rho(t). \end{aligned} \quad (\text{S83})$$

Here, we have assumed that the bare-cavity mode and the mechanical mode are coupled to two independent thermal reservoirs. The effective Hamiltonian H_{eff} in Eq. (S83) is given in Eq. (S22) in Sec. , and for convenience, is reproduced here

$$H_{\text{eff}} = \Delta_s a_s^\dagger a_s + \Delta_m b^\dagger b + g_{\text{DCE}} (a_s^2 b^\dagger + a_s^\dagger b) + \frac{1}{2} F (b + b^\dagger). \quad (\text{S84})$$

In the limit $\Omega \ll \Delta$, the squeezing parameter r is approximated to

$$r = \frac{1}{4} \ln \left(\frac{\Delta + \Omega}{\Delta - \Omega} \right) \simeq \frac{\Omega}{2\Delta}, \quad (\text{S85})$$

which, in turn, gives

$$a_s = \cosh(r) a + \sinh(r) a^\dagger \simeq a, \quad (\text{S86})$$

due to $\cosh(r) \simeq 1 \gg \sinh(r) \simeq \Omega/2\Delta$. We find that, in this limit, the SCM a_s is reduced to the bare cavity mode a . This is because the detuned, weak two-photon driving Ω leads to a weak squeezing of the a mode, such that the a mode approximately remains unchanged. In addition, by appropriately choosing a small (but not too small) r , the standard optomechanical coupling in the form $g_{\text{OM}} a_s^\dagger a_s (b + b^\dagger)$ can still be neglected, compared to the parametric coupling in Eq. (S84). In this case, the mechanical mode b is effectively, parametrically coupled to the mode a and, as a result, the Hamiltonian H_{eff} is approximated to

$$H_{\text{eff}} \simeq \tilde{H}_{\text{eff}} = \Delta_s a^\dagger a + \Delta_m b^\dagger b + g_{\text{DCE}} (a^2 b^\dagger + a^\dagger b) + \frac{1}{2} F (b + b^\dagger), \quad (\text{S87})$$

where

$$g_{\text{DCE}} = \frac{1}{2} g_0 \sinh(2r) \simeq \frac{g_0 \Omega}{2\Delta}. \quad (\text{S88})$$

The unitary evolution under \tilde{H}_{eff} can convert one mechanical phonon into two intracavity photons, as shown in Fig. S10. This figure also shows that the dynamics under the effective Hamiltonian \tilde{H}_{eff} can exactly describe the dynamics under the full Hamiltonian H in Eq. (1) in the main article. Comparing \tilde{H}_{eff} in Eq. (S87) with H_{eff} in Eq. (S84), we can further find that the DCE is mapped from the a_s mode onto the a mode, which enables one to observe the DCE more directly in the laboratory frame. Note that such a map (that is, the approximate relation $a_s \simeq a$) can be made more accurate by decreasing the ratio Ω/Δ , but at the expense of the DCE radiation strength.

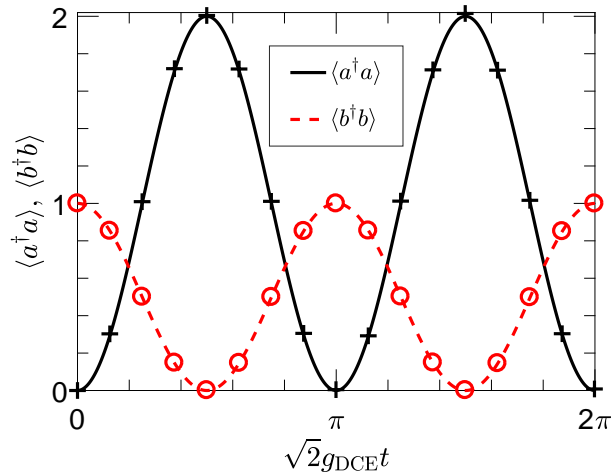


FIG. S10. Parametric energy conversion between the mechanical motion and the bare-cavity field. Under the unitary evolution, one mechanical phonon can simultaneously excite two bare-cavity photons. Curves are obtained from the Hamiltonian in Eq. (S87) and symbols from the full Hamiltonian in Eq. (1) in the main article. They show an excellent agreement. Here, the initial state is $|\tilde{0}, 1\rangle$, where the first number in the ket refers to the number of photons in the bare-cavity mode and the second to the number of mechanical phonons, and we set $\Omega/\Delta = 0.1$, $\omega_m = \omega_d = 2\omega_s = 10^3 g_0$, and $F = \gamma_m = \kappa = 0$.

Therefore, the master equation is given by

$$\begin{aligned} \frac{d}{dt}\rho(t) = & i \left[\rho(t), \tilde{H}_{\text{eff}} \right] - \frac{\kappa}{2} \mathcal{L}(a) \rho(t) \\ & - \frac{\gamma_m}{2} (n_{\text{th}} + 1) \mathcal{L}(b) \rho(t) - \frac{\gamma_m}{2} n_{\text{th}} \mathcal{L}(b^\dagger) \rho(t). \end{aligned} \quad (\text{S89})$$

In the $\Omega \ll \Delta$ limit, we find that the squeezing-induced noise, which includes thermal noise $\propto \sinh^2(r)$ and two-photon correlation noise $\propto \sinh(2r)$, is strongly suppressed, even when there is no squeezed-vacuum bath. Furthermore, we find that this master equation for the a mode is the same as given in Eq. (S23) for the a_s mode. Therefore, in the original laboratory frame, we can observe DCE signatures similar to what we have already given before for the a_s mode in the squeezed frame. According to the master equation in Eq. (S89), it is seen that the photons generated inside the cavity completely arise from the vacuum radiation or the mechanical motion, and thus all of them are the DCE photons. This is owing to the negligible background noise in the $\Omega \ll \Delta$ limit.

In Fig. S11 we plot the steady-state intracavity photon number $\langle a^\dagger a \rangle_{\text{ss}}$ and the equal-time second-order correlation function

$$g^{(2)}(0) = \frac{\langle a^{\dagger 2} a^2 \rangle_{\text{ss}}}{\langle a^\dagger a \rangle_{\text{ss}}^2} \quad (\text{S90})$$

versus the mechanical driving F . It is seen that the dynamics driven by the master equation in Eq. (S89) is in excellent agreement with that driven by the master equation in Eq. (S83). We also find from Fig. S11(a) that the number, $\langle a^\dagger a \rangle_{\text{ss}}$, of DCE photons increases with the driving F , as expected. For realistic parameters $g_0 = 10\gamma_m$, $\Omega/\Delta = 0.1$, and $\kappa = 500\gamma_m$, we can obtain $\langle a^\dagger a \rangle_{\text{ss}} \simeq 1.8 \times 10^{-3}$ for $F = 15\gamma_m$. A typical cavity linewidth of $\kappa/2\pi = 2$ MHz could result in an output-photon flux $\simeq 2.0 \times 10^4$ photons per second. This radiation strength is much larger than the dark count rate of a common single-photon detector, and is therefore sufficient to be detected by using single-photon detection devices. Furthermore, we find from Fig. S11(b) that the $g^{(2)}(0)$ correlation is very large, corresponding to strong photon bunching. This reflects that the photons are emitted in pairs through the DCE process.

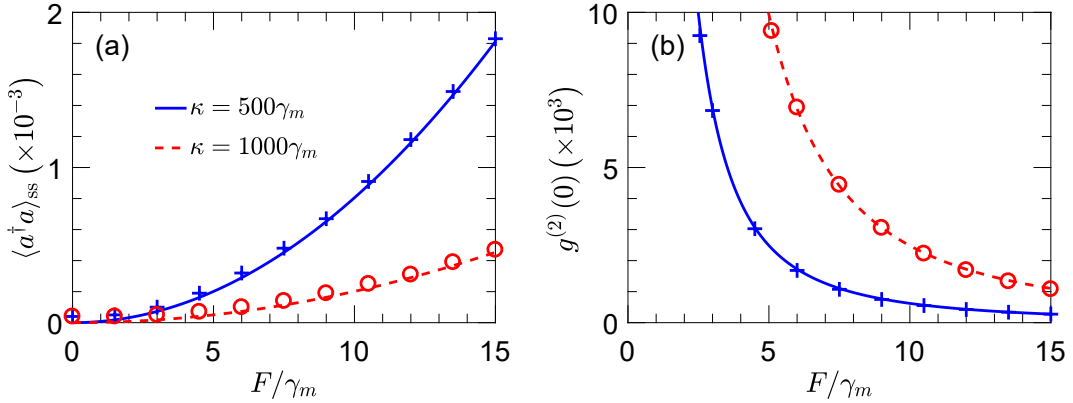


FIG. S11. (a) Photon number $\langle a^\dagger a \rangle_{\text{ss}}$ and (b) correlation function $g^{(2)}(0)$ versus the mechanical driving F for $\kappa = 500\gamma_m$, and $1000\gamma_m$. Curves are obtained from the master equation in Eq. (S89) and symbols from the master equation in Eq. (S83). They show an excellent agreement. For both plots, we have assumed that $g_0 = 10\gamma_m$, $\Omega/\Delta = 0.1$, $\omega_m = \omega_d = 2\omega_s$, and $n_{\text{th}} = 0$.

POSSIBLE IMPLEMENTATIONS WITH SUPERCONDUCTING QUANTUM CIRCUITS

Our scheme to implement the DCE is based on a generic optomechanical system, and at the same time, does not require an ultra-high-frequency mechanical resonator and an ultrastrong single-photon coupling between light and mechanical motion. Therefore, we can expect that it can be implemented in various physical systems. In this section, as an example, we discuss in detail a possible implementation with superconducting circuits and, in particular, we refer to the experimental superconducting quantum circuit of Ref. [S14], described by the standard optomechanical coupling of the form $a^\dagger a (b + b^\dagger)$.

A standard LC circuit consists of a capacitor (e.g., with capacitance C_0) and an inductor (e.g., with inductance L_0), as shown in Fig. S12(a). Its Hamiltonian is expressed in terms of the capacitor charge Q and the inductor current I as

$$H_0 = \frac{\Phi^2}{2L_0} + \frac{1}{2}L_0\omega_0^2Q^2, \quad (\text{S91})$$

where $\Phi = L_0I$ is the magnetic flux through the inductor, and $\omega_0 = 1/\sqrt{L_0C_0}$ is the fundamental frequency of the circuit. After quantization, the charge Q and the flux Φ represent a pair of canonically conjugate variables, which obey the commutation relation $[Q, \Phi] = i\hbar$. Upon introducing a canonical transformation,

$$Q = \frac{1}{2}\sqrt{2\hbar\omega_0C_0}(a + a^\dagger), \quad \text{and} \quad \Phi = \frac{1}{2i}\sqrt{2\hbar\omega_0L_0}(a - a^\dagger), \quad (\text{S92})$$

the Hamiltonian H_0 becomes

$$H_0 = \hbar\omega_0 a^\dagger a. \quad (\text{S93})$$

Here, we have subtracted the constant zero-point energy $\hbar\omega_0/2$. Such an LC circuit thus behaves as a single-mode microwave cavity, with ω_0 being the cavity frequency, and with a (a^\dagger) being the annihilation (creation) operator of the cavity mode.

As demonstrated in Ref. [S14], when the capacitance C_0 in Fig. S12(a) is modulated by the mechanical motion of a micromechanical membrane, the mechanical motion can couple to the cavity mode. In this manner, the capacitance C_0 becomes

$$C_0 \mapsto C_x = \frac{C_0}{1 + x/d}, \quad (\text{S94})$$

where x is the displacement of the membrane, and d is the distance between the conductive plates of the capacitor. To parametrically squeeze the cavity mode, we further add an additional and electrically tunable capacitor into such an experimental setup. The LC circuit is shown in Fig. S12(b). Here, we assume the capacitance of the additional capacitor to be

$$C_t = C_0 + \Delta C \cos(\omega_L t), \quad (\text{S95})$$

where ω_L is the modulation frequency, and $\Delta C \ll C_0$. The total capacitance is thus given by $C_{\text{total}} = C_t + C_x$. Note that, in the absence of both mechanical motion and cosine modulation, the total capacitance is equal to $2C_0$, and as a result, the resonance frequency of the bare LC cavity, shown in Fig. S12(b), is $\omega_c = \omega_0/\sqrt{2}$, rather than $= \omega_0$. When both mechanical motion and cosine modulation are present, the cavity frequency ω_c is modulated as

$$\omega_c \mapsto \omega'_c = \frac{1}{\sqrt{L_0 C_{\text{total}}}} = \frac{\omega_0}{\sqrt{1 + \frac{\Delta C}{C_0} \cos(\omega_L t) + \frac{1}{1+x/d}}}. \quad (\text{S96})$$

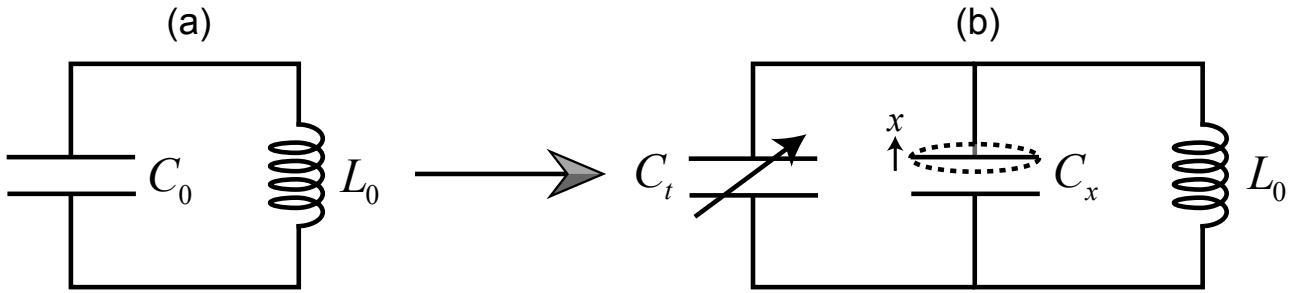


FIG. S12. (a) A standard LC circuit consisting of a capacitor (C_0) and an inductor (L_0). This circuit behaves as a single-mode microwave cavity. (b) An LC circuit used to implement the DCE. Its capacitor (C_x) is modulated by the mechanical motion, e.g., of a micromechanical membrane, and this results in a standard optomechanical coupling between light and mechanics. Meanwhile, the use of the electrically tunable capacitor (C_t) can parametrically drive and squeeze the cavity mode.

In the limit $\{\Delta C/C_0, x/d\} \ll 1$, we can expand ω'_c , up to first order, to have

$$\omega'_c \simeq \omega_c \left[1 - \frac{\Delta C}{4C_0} \cos(\omega_L t) + \frac{x}{4d} \right]. \quad (\text{S97})$$

The Hamiltonian describing the cavity mode of the LC circuit in Fig. S12(b) is then given by

$$H_c = \frac{\Phi^2}{2L_0} + \frac{1}{2}L_0\omega_c^2 \left[1 - \frac{\Delta C}{2C_0} \cos(\omega_L t) + \frac{x}{2d} \right] Q^2. \quad (\text{S98})$$

Using the canonical transformation in Eq. (S92), but with ω_0 replaced by ω_c , the Hamiltonian H_c is reduced to

$$H_c = \hbar\omega_c a^\dagger a - \hbar g_0 a^\dagger a (b + b^\dagger) + \frac{1}{2}\hbar\Omega [\exp(i\omega_L t) a^2 + \exp(-i\omega_L t) a^{\dagger 2}], \quad (\text{S99})$$

where b (b^\dagger) is the annihilation (creation) operator of the mechanical mode, $g_0 = -\omega_c x_{\text{zpf}}/4d$ is the single-photon optomechanical coupling, x_{zpf} is the zero-point fluctuation of the mechanical resonator, $\Omega = -\omega_c \Delta C/8C_0$ is the amplitude of the two-photon driving, and ω_L is its frequency. Here, we have made the rotating-wave approximation, and we have also replaced $x \mapsto x_{\text{zpf}}(b + b^\dagger)$. After including the free Hamiltonian of the mechanical resonator, the full Hamiltonian, in a rotating frame at $\omega_L/2$, becomes ($\hbar = 1$)

$$H = \omega_m b^\dagger b + \Delta a^\dagger a - g_0 a^\dagger a (b + b^\dagger) + \frac{1}{2}\Omega (a^2 + a^{\dagger 2}), \quad (\text{S100})$$

where ω_m is the frequency of the mechanical mode, and $\Delta = \omega_c - \omega_L/2$. The Hamiltonian in Eq. (S100) is exactly the one applied by us in this work.

A squeezed-vacuum reservoir coupled to the cavity mode can be realized directly using the LC circuit in Fig. S12(a), but the constant capacitance C_0 needs to be replaced by a tunable capacitance C_t . By following the same recipe as above, the corresponding Hamiltonian is then given by

$$H_r = \Delta_0 a^\dagger a + \frac{1}{2}\Omega_0 (a^2 + a^{\dagger 2}), \quad (\text{S101})$$

where $\Delta_0 = \omega_0 - \omega_L/2$, and $\Omega_0 = -\omega_0 \Delta C/8C_0$. The canonical transformation used here is the same as given in Eq. (S92). When the input field of the cavity is in the vacuum, we can obtain a squeezed-vacuum field at the output port, according to the input-output relation.

In addition to the LC circuit, the squeezed-vacuum reservoir can also be generated by a Josephson parametric amplifier, as experimentally demonstrated in Refs. [S15, S16]. In particular, a squeezing bandwidth of up to ~ 10 MHz was reported in Ref. [S15]. This is sufficient to fulfil the large-bandwidth requirement of the reservoir.

-
- [S1] X.-Y. Lü, Y. Wu, J. R. Johansson, H. Jing, J. Zhang, and F. Nori, “Squeezed Optomechanics with Phase-Matched Amplification and Dissipation,” *Phys. Rev. Lett.* **114**, 093602 (2015).
- [S2] M. Lemonde, N. Didier, and A. A. Clerk, “Enhanced nonlinear interactions in quantum optomechanics via mechanical amplification,” *Nat. Commun.* **7** (2016).
- [S3] W. Qin, A. Miranowicz, P.-B. Li, X.-Y. Lü, J. Q. You, and F. Nori, “Exponentially Enhanced Light-Matter Interaction, Cooperativities, and Steady-State Entanglement Using Parametric Amplification,” *Phys. Rev. Lett.* **120**, 093601 (2018).
- [S4] C. Leroux, L. C. G. Govia, and A. A. Clerk, “Enhancing Cavity Quantum Electrodynamics via Antisqueezing: Synthetic Ultrastrong Coupling,” *Phys. Rev. Lett.* **120**, 093602 (2018).
- [S5] M. O. Scully and M. S. Zubairy, *Quantum Optics* (Cambridge University Press, Cambridge, 1997).
- [S6] J. R. Johansson, P. D. Nation, and F. Nori, “Qutip: An open-source Python framework for the dynamics of open quantum systems,” *Comput. Phys. Commun.* **183**, 1760–1772 (2012).
- [S7] J. R. Johansson, P. D. Nation, and F. Nori, “Qutip 2: A Python framework for the dynamics of open quantum systems,” *Comput. Phys. Commun.* **184**, 1234–1240 (2013).
- [S8] J. R. Johansson, G. Johansson, C. M. Wilson, and F. Nori, “Dynamical Casimir effect in superconducting microwave circuits,” *Phys. Rev. A* **82**, 052509 (2010).
- [S9] R. Stassi, A. Ridolfo, O. Di Stefano, M. J. Hartmann, and S. Savasta, “Spontaneous Conversion from Virtual to Real Photons in the Ultrastrong-Coupling Regime,” *Phys. Rev. Lett.* **110**, 243601 (2013).
- [S10] V. Macrì, A. Ridolfo, O. Di Stefano, A. F. Kockum, F. Nori, and S. Savasta, “Nonperturbative Dynamical Casimir Effect in Optomechanical Systems: Vacuum Casimir-Rabi Splittings,” *Phys. Rev. X* **8**, 011031 (2018).

- [S11] S. Butera and I. Carusotto, “Mechanical back-reaction effect of the dynamical Casimir emission,” [arXiv preprint arXiv:1810.11281](#) (2018).
- [S12] D. Sarchi, I. Carusotto, M. Wouters, and V. Savona, “Coherent dynamics and parametric instabilities of microcavity polaritons in double-well systems,” *Phys. Rev. B* **77**, 125324 (2008).
- [S13] O. Kyriienko, T. C. H. Liew, and I. A. Shelykh, “Optomechanics with Cavity Polaritons: Dissipative Coupling and Unconventional Bistability,” *Phys. Rev. Lett.* **112**, 076402 (2014).
- [S14] J. D. Teufel, T. Donner, D. Li, J. W. Harlow, M. S. Allman, K. Cicak, A. J. Sirois, J. D. Whittaker, K. W. Lehnert, and R. W. Simmonds, “Sideband cooling of micromechanical motion to the quantum ground state,” *Nature (London)* **475**, 359 (2011).
- [S15] K. W. Murch, S. J. Weber, K. M. Beck, E. Ginossar, and I. Siddiqi, “Reduction of the radiative decay of atomic coherence in squeezed vacuum,” *Nature (London)* **499**, 62–65 (2013).
- [S16] D. M. Toyli, A. W. Eddins, S. Boutin, S. Puri, D. Hover, V. Bolkhovsky, W. D. Oliver, A. Blais, and I. Siddiqi, “Resonance Fluorescence from an Artificial Atom in Squeezed Vacuum,” *Phys. Rev. X* **6**, 031004 (2016).